Virology 462-463 (2014) 166-174

Contents lists available at ScienceDirect

Virology

journal homepage: www.elsevier.com/locate/yviro

Rab18 is required for viral assembly of hepatitis C virus through trafficking of the core protein to lipid droplets

Hiromichi Dansako [a], Hiroki Hiramoto [a], Masanori Ikeda [a], Takaji Wakita [b], Nobuyuki Kato [a,*]

[a] Department of Tumor Virology, Okayama University Graduate School of Medicine, Dentistry and Pharmaceutical Sciences, 2-5-1 Shikata-cho, Kita-ku, Okayama 700-8558, Japan
[b] Department of Virology II, National Institute of Infectious Disease, 1-23-1 Toyama, Shinjuku-ku, Tokyo 162-8640, Japan

ARTICLE INFO

Article history:
Received 14 February 2014
Returned to author for revisions
11 March 2014
Accepted 14 May 2014

Keywords:
Hepatitis C virus
Rab18
Viral assembly
Lipid droplet
Core protein
RNA replication

ABSTRACT

During persistent infection of HCV, the HCV core protein (HCV-JFH-1 strain of genotype 2a) is recruited to lipid droplets (LDs) for viral assembly, but the mechanism of recruitment of the HCV core protein is uncertain. Here, we demonstrated that one of the Ras-related small GTPases, Rab18, was required for trafficking of the core protein around LDs. The knockdown of Rab18 reduced intracellular and extracellular viral infectivity, but not intracellular viral replication in HCV-JFH-1-infected RSc cells (an HuH-7-derived cell line). Exogenous expression of Rab18 increased extracellular viral infectivity almost two-fold. Furthermore, Rab18 was co-localized with the core protein in HCV-JFH-1-infected RSc cells, and the knockdown of Rab18 blocked recruitment of the HCV-JFH-1 core protein to LDs. These results suggest that Rab18 has an important role in viral assembly through the trafficking of the core protein to LDs.

Introduction

Hepatitis C virus (HCV) is an enveloped positive single-stranded RNA virus belonging to the *Flaviviridae* family (Choo et al., 1989). The HCV genome encodes a large polyprotein precursor of approximately 3000 amino acid (aa) residues, which is cleaved co- and post-translationally into at least ten proteins in the following order: core, envelope 1 (E1), E2, p7, nonstructural protein 2 (NS2), NS3, NS4A, NS4B, NS5A, and NS5B (Kato, 2001). Persistent HCV infection in the liver causes chronic hepatitis, and then highly progresses to liver cirrhosis and hepatocellular carcinoma (Ohkoshi et al., 1990). Therefore, the elimination of HCV RNA by the anti-HCV reagents such as interferon is necessary to block the progression of liver diseases such as liver cirrhosis and hepatocellular carcinoma. To date, the HCV-JFH-1 strain (genotype 2a) has mainly been used to study the complete life cycle of HCV worldwide. In HCV-JFH-1-infected human hepatoma HuH-7 cells, viral replication intermediate, double-stranded RNA, is detected adjacent to the membranes of the endoplasmic reticulum (ER) (Targett-Adams et al., 2008). In addition, the HCV replication complex is formed on a detergent-resistant membrane (Shi et al., 2003). These results suggest that HCV RNA replication occurs on lipid rafts and the membranous web at the cytosolic side of the ER. Following viral replication, the HCV core protein matures through the translation of a large polyprotein precursor from HCV RNA and then the processing by signal peptide peptidase. The matured HCV-JFH-1 core protein has been shown to be trafficked to lipid droplets (LDs) for viral assembly (Miyanari et al., 2007).

LDs are important organelles for lipid metabolism. LDs are covered by a phospholipid monolayer, and accumulate excessive neutral lipids such as triglycerides. A proteomics analysis revealed that a number of host factors are associated with LDs (Brasaemle et al., 2004). These host factors are required for acquisition, storage, lipolysis, transport and/or release of lipids, respectively. The first of these LD-associated factors to be identified were members of the PAT family of proteins, including perilipin (PLIN), ADRP (adipose differentiation-related protein; also named adipophilin or PLIN2), and TIP47 (also named PLIN3). PLIN is expressed only in adipocytes and steroidogenic cells, whereas ADRP and TIP47 are expressed in various cell types. ADRP and TIP47 have similar sequences and three-dimensional structures (Hickenbottom et al., 2004), but their intracellular distributions in HuH-7 cells are different (Ohsaki et al., 2006). ADRP localizes exclusively to the surface of LDs in HuH-7 cells, whereas only some of total TIP47 localizes to the LD surface in this cell line. During viral assembly, the core protein is trafficked to ADRP on LDs (Counihan et al., 2011). ADRP is displaced from the surface of LDs to the cytoplasm by the core protein, and then subjected to degradation (Boulant et al., 2008). These displacements

* Corresponding author. Fax: +81 86 235 7392.
E-mail address: nkato@md.okayama-u.ac.jp (N. Kato).

http://dx.doi.org/10.1016/j.virol.2014.05.017
0042-6822/

of ADRP also cause the redistribution of LDs around the nucleus (Boulant et al., 2008). These observations imply that the core protein may increase the probability of an interaction between the sites of viral replication at the ER and viral assembly at the LDs. However, the precise mechanism of intracellular trafficking of the core protein to ADRP on LDs is still uncertain.

A family of Ras-related small GTPases plays an important role in the membrane trafficking between organelles such as the ER, Golgi, early/late endosomes, LDs, and so on (Hutagalung and Novick, 2011). One of the Ras-related small GTPases, Rab18, is required for membrane trafficking between the ER and Golgi (Dejgaard et al., 2008). On the other hand, Rab18 is an LD-associated protein, and the ectopic expression of Rab18 induces the close apposition of LDs to ER membranes through the reduction of ADRP (Ozeki et al., 2005). These observations imply that Rab18 may be required for membrane trafficking through the redistribution of LDs around the ER. Recently, Salloum et al. reported that Rab18 bound HCV-JFH-1 NS5A and may have promoted the interaction between sites of viral replication and LDs in HCV-Jc1-infected Huh7.5.1 cells (Salloum et al., 2013). However, HCV-Jc1 is an intragenotypic recombinant encoding core to NS2 from the HCV-J6 strain (genotype 2a) in the context of HCV-JFH-1, and does not exist in nature. In addition, although HCV-Jc1 was shown to be more robust in the release of viral particles than HCV-JFH-1, the HCV-J6 core protein did not associate with LDs (Shavinskaya et al., 2007). On the other hand, the HCV-JFH-1 core protein does associate with LDs, and LD-associated core proteins recruit HCV NS protein from the ER to LDs (Miyanari et al., 2007). These results imply that HCV-Jc1 may release viral particles via an intracellular organelle distinct from the LDs. Therefore, we hypothesized that Rab18 first trafficked the HCV-JFH-1 core protein and subsequently NS5A to LD. To prove this hypothesis, we examined the association of the HCV-JFH-1 core protein with LDs and the levels of viral assembly in Rab18-knockdown cells.

Here, we show that Rab18 is required for trafficking of the HCV-JFH-1 core protein to LDs and the subsequent assembly of HCV. Rab18 may be involved in the maturation of viral particles through membrane trafficking of the HCV-JFH-1 core protein from the sites of viral replication at the ER to viral assembly at the LDs in human hepatocytes.

Results

RSc cells show higher viral productivity than Huh7.5 cells

To date, human hepatoma HuH-7 cells have mainly been used to study the complete life cycle of HCV in studies worldwide. One of the sublines of HuH-7 cells, Huh7.5, is used in many laboratories for its high susceptibility to infection with the HCV-JFH-1 strain (genotype 2a). On the other hand, we have previously established several types of HCV RNA-replicating cells (genotype 1b, O strain), such as sO cells (Kato et al., 2003, sub-genomic HCV RNA), O cells (Ikeda et al., 2005, genome-length HCV RNA), and OR6 cells (Ikeda et al., 2006, genome-length HCV RNA-encoding renilla luciferase) derived from HuH-7 cells, and their "cured" cells (sOc (Kato et al., 2003), Oc (Ikeda et al., 2005), OR6c (Ikeda et al., 2006), respectively) by the elimination of HCV RNA (Fig. 1A). The cured cell lines have been reported to increase the permissiveness of HCV (Blight et al., 2002). We also previously reported that Oc cells showed higher permissiveness of HCV than sOc cells (Abe et al., 2007). RSc cells are one of our cured cell lines derive from OR6c cells, and have mainly been used to study the complete life cycle of HCV in our laboratory (Ariumi et al., 2007, 2008; Kato et al., 2009). However, we have no information on viral susceptibility of our cured cell lines to HCV-JFH-1 infection. To identify which of our cured cell lines would be most useful for the infection with HCV-JFH-1, we first compared the amounts of LDs by two methods, i.e., a confocal microscope and flow cytometry. The LDs were stained with BODIPY493/503 and observed under a confocal microscope. In our cured cells (sOc, Oc, OR6c, and RSc cells), the numbers rather than the sizes of LDs have increased compared to HuH-7 cells (Fig. 1B). In addition, the mean fluorescence intensity of BODIPY493/503-stained cells has increased by the enhancements of the numbers of LDs (Fig. 1C). These qualitative and quantitative analyses revealed that our cured cells (sOc, Oc, OR6c, and RSc cells) formed higher levels of LDs than HuH-7 and Huh7.5 cells (Fig. 1B and C). Interestingly, irrespective of the quantitative difference of LDs, the levels of viral replication at 72 h after the viral inoculation of HCV-JFH-1 were comparable between each of our cured cell lines and Huh7.5 cells, but not between each of the cured cell lines and HuH-7 cells (Fig. 1D). Moreover, the time-course analysis showed that the capacities of HCV RNA replication were almost comparable between RSc and Huh7.5 cells (Fig. 1E). These results suggest that the levels of HCV RNA replication do not depend on the amount of LDs. Next, to compare the levels of viral assembly and viral productivity between RSc and Huh7.5 cells, we examined the infectivity of the cell lysates (intracellular infectivity) and the supernatants (extracellular infectivity) derived from both lines of HCV-JFH-1-infected cells. The intracellular and extracellular infectivities of HCV-JFH-1-infected RSc cells were significantly higher than those of HCV-JFH-1-infected Huh7.5 cells (Fig. 1F). These results suggest that RSc cells possess higher viral productivity in response to infection with HCV-JFH-1 than Huh7.5 cells.

Rab18 is required for viral production, but not viral RNA replication

As the first step of viral assembly, the HCV-JFH-1 core protein displaces ADRP from the surface of LDs to the cytoplasm (Boulant et al., 2008; Counihan et al., 2011). In the present study, we tried to clarify how the core protein is trafficked to LDs by using RSc and Huh7.5 cells. It has been reported that Rab18, one of the Ras-related small GTPase family members, induces the close apposition of LDs to ER membranes through the reduction of ADRP (Ozeki et al., 2005). Based on these previous findings, we hypothesized that Rab18 is required for trafficking of the HCV-JFH-1 core protein to LDs. To prove this hypothesis, we first examined the expression levels of Rab18 in RSc and Huh7.5 cells. The expression levels of Rab18 were almost comparable between RSc cells and Huh7.5 cells at both the transcript (Fig. 2A) and protein levels (Fig. 2B). Two other members of the Ras-related small GTPases, Rab5 and Rab7, were also present at almost the same levels in RSc and Huh7.5 cells. We next examined the effect of the knockdown of Rab18 against HCV replication in RSc cells. The knockdown of Rab18 (Fig. 2C) had no effect on the RNA replication step (Fig. 2D). Rab18-knockdown Huh7.5 cells and genome-length HCV RNA-replicating O cells (Kato et al., 2009) also showed similar results (Fig. 2E and F, Supplemental Fig. S1A and B). However, we found that the knockdown of Rab18 caused a significant decrease in viral productivity in both RSc and Huh7.5 cells (Fig. 2G). In addition, the knockdown of ADRP (Supplemental Fig. S2A) also decreased viral productivity rather than HCV RNA replication (Supplemental Fig. S2B). Furthermore, we demonstrated that the overexpression of Rab18 (Fig. 2H) recovered the viral productivity (Fig. 2I) rather than viral RNA replication (Fig. 2J). From these results, we conclude that Rab18 is required for viral production of HCV.

Rab18 is required for viral assembly through the trafficking of the HCV-JFH-1 core protein to LDs

To clarify whether Rab18 is required for the viral assembly step, we first examined the localization of Rab18 and the HCV core protein in HCV-JFH-1-infected cells. The results revealed that Rab18

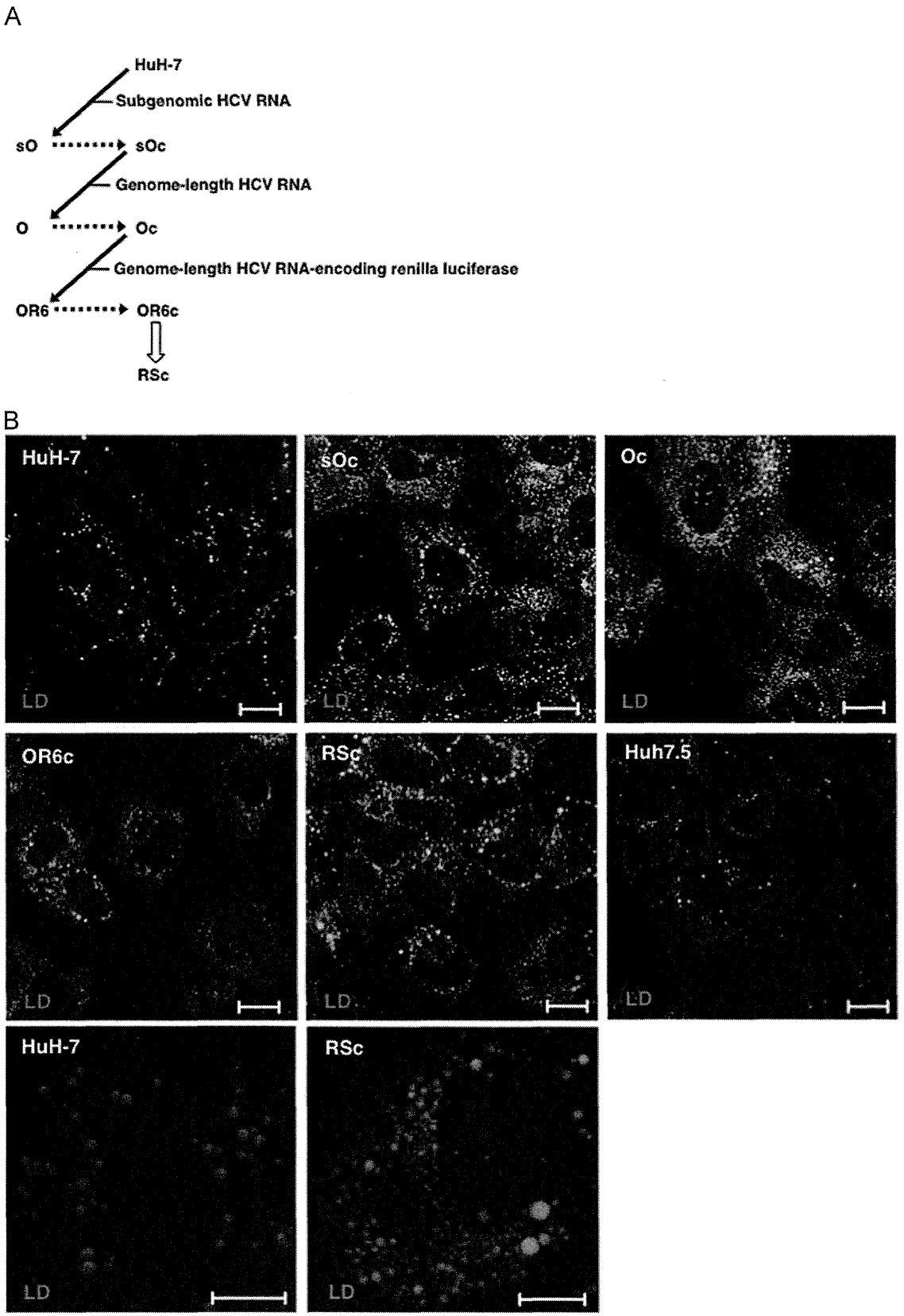

Fig. 1. RSc cells possess higher viral productivity in response to the infection with HCV-JFH-1 than Huh7.5 cells. (A) Outline for the establishment of our HCV RNA-replicating cells and their "cured" cells. Our HCV RNA-replicating cells (sO, O, and OR6 cells) are independently established by the transfection of HCV RNA into HuH-7 or cured cells (sOc or Oc cells) as previously reported (Ikeda et al., 2005, 2006; Kato et al., 2003). To prepare the cured cells, HCV RNA was eliminated from HCV RNA-replicating cells by the interferon treatment. RSc cells are one of the sublines of OR6c cells. The arrows with solid and dashed lines show the transfection of HCV RNA and the interferon treatment, respectively. (B) Visualization of LD under a confocal microscope. The panels show the fluorescence of LD by staining with BODIPY493/503. Bars, 20 μm. (C) Measurement of the mean fluorescence intensity of BODIPY493/503-stained cells by a flow cytometer. These levels were calculated relative to the level in HuH-7 cells, which was set at 1. (D) Quantitative RT-PCR analysis of HCV RNA in our cured cells 72 h after infection with HCV-JFH-1. Total RNA extracted from the cells was subjected to quantitative RT-PCR analysis. The experiments were performed in at least triplicate. (E) Time-course analysis of HCV RNA in RSc and Huh7.5 cells after infection with HCV-JFH-1. Total RNA was extracted from HCV-JFH-1-infected cells at each time point. (F) Quantitative RT-PCR analysis of HCV RNA in Huh7.5 cells 72 h after infection with intracellular (left panel) and extracellular (right panel) HCV-JFH-1. As intracellular or extracellular HCV-JFH-1, the lysate or the supernatant was recovered from RSc cells (designated J-RSc in the figure) and Huh7.5 cells (designated J-Huh7.5) 24 h after infection with HCV-JFH-1.

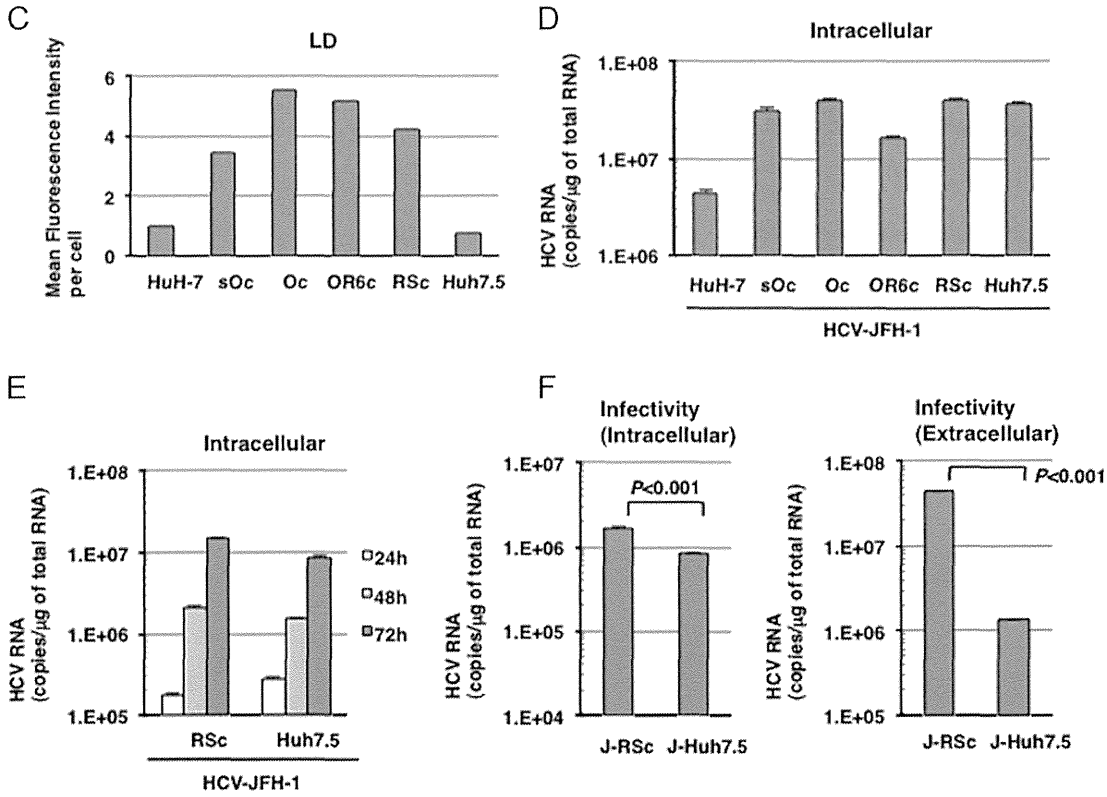

Fig. 1. (*continued*)

was co-localized with the core protein in HCV-JFH-1-infected RSc and Huh7.5 cells (Fig. 3A). We previously reported that the core protein was not recruited to LDs in O cells, from which no infectious virus was produced (data not shown). In fact, in contrast to HCV-JFH-1-infected RSc and Huh7.5 cells, co-localization of Rab18 and the core protein was not observed in O cells (Fig. 3B), although the expression of Rab18 were almost comparable levels among these cell lines (Supplemental Fig. S1C). We next examined the infectivity of intracellular viral particles in HCV-JFH-1-infected RSc siRab18 cells. The results revealed that the knockdown of Rab18 inhibited 90% of the production of intracellular viral particles (Fig. 3C) and the recruitment of the core protein to LDs (Fig. 3D). However, the knockdown of Rab4 (early endosome marker), other Ras-related small GTPase family member, inhibited only 40% of the production of intracellular viral particles (Supplemental Fig. S3C). These results suggest that Rab18 is particularly required for viral assembly through the trafficking of the core protein to LDs. Rab18 may be involved in the maturation of viral particles through membrane trafficking of the core protein from the ER to LDs.

Discussion

Previous proteomics analysis showed that a number of host factors were associated with LDs (Brasaemle et al., 2004). These LD-associated proteins may be required for the life cycle of HCV as well as the metabolism of lipids. During viral production, the HCV core protein is recruited to LDs in HCV-JFH-1-infected cells (Miyanari et al., 2007). In the present study, we suggest that one of the LD-associated proteins, Rab18, is required for trafficking of the HCV core protein to LDs and subsequent viral assembly.

The HCV core protein consists of three domains (domains 1, 2, and 3). Domain 2 (aa 118–173) contains two proline residues at aa positions 138 and 143, and a YATG sequence ranging from aa positions 164–167 that is essential for the association with LDs (Hope et al., 2002). These are conserved in both the JFH-1 strain (genotype 2a) and O strain (genotype 1b). However, the core protein was associated with LDs in HCV-JFH-1-infected RSc cells (Fig. 3D), but not in genome-length HCV RNA-replicating O cells (Kato et al., 2009). Matto et al. found that there were two morphologically distinct populations of the core protein (the ring-like and the dot-like pattern) in genome-length HCV RNA (genotype 1b)-replicating cells (Matto et al., 2004). The ring-like core protein was associated with LDs, and the dot-like core protein was associated with the detergent-resistant membranes and the lipid rafts essential for viral replication (Matto et al., 2004). We previously demonstrated that the core protein of the O strain showed a dot-like pattern (Kato et al., 2009), and that infectious virus was not produced from O cells (data not shown). In contrast to the core protein of the JFH-1 strain, the core protein of the O strain was not trafficked to LDs, and may have remained at the detergent-resistant membranes and the lipid rafts.

We also demonstrated that the core protein was co-localized with Rab18 in HCV-JFH-1-infected RSc cells, but not in O cells (Fig. 3B). In addition, we demonstrated that the knockdown of Rab18 did not inhibit HCV RNA replication in O cells as well as HCV-JFH-1-infected RSc cells (Supplemental Figs. S1B and S3B). However, in contrast to our results, Salloum et al. have previously observed that the knockdown of Rab18 inhibited HCV RNA replication in OR6 cells (Salloum et al., 2013). From these results, we speculate the clonality of HuH-7 cells as one of causes of this discrepancy. On the other hand, it also remains the possibility that the induction of IFN-β by shRNA reduced HCV RNA replication. Kenworthy et al. has previously reported that the introduction of shRNA by lentiviral vector may induce IFN-β (Kenworthy et al., 2009). Rab18 knockdown cells in the Salloum's paper were generated by the introduction of shRNA using lentiviral vector. In addition, Rab18 overexpression did not enhance HCV RNA replication in OR6 cells (Salloum et al., 2013). Another proteomic analysis suggested that Rab18 is upregulated in the lipid raft fraction of

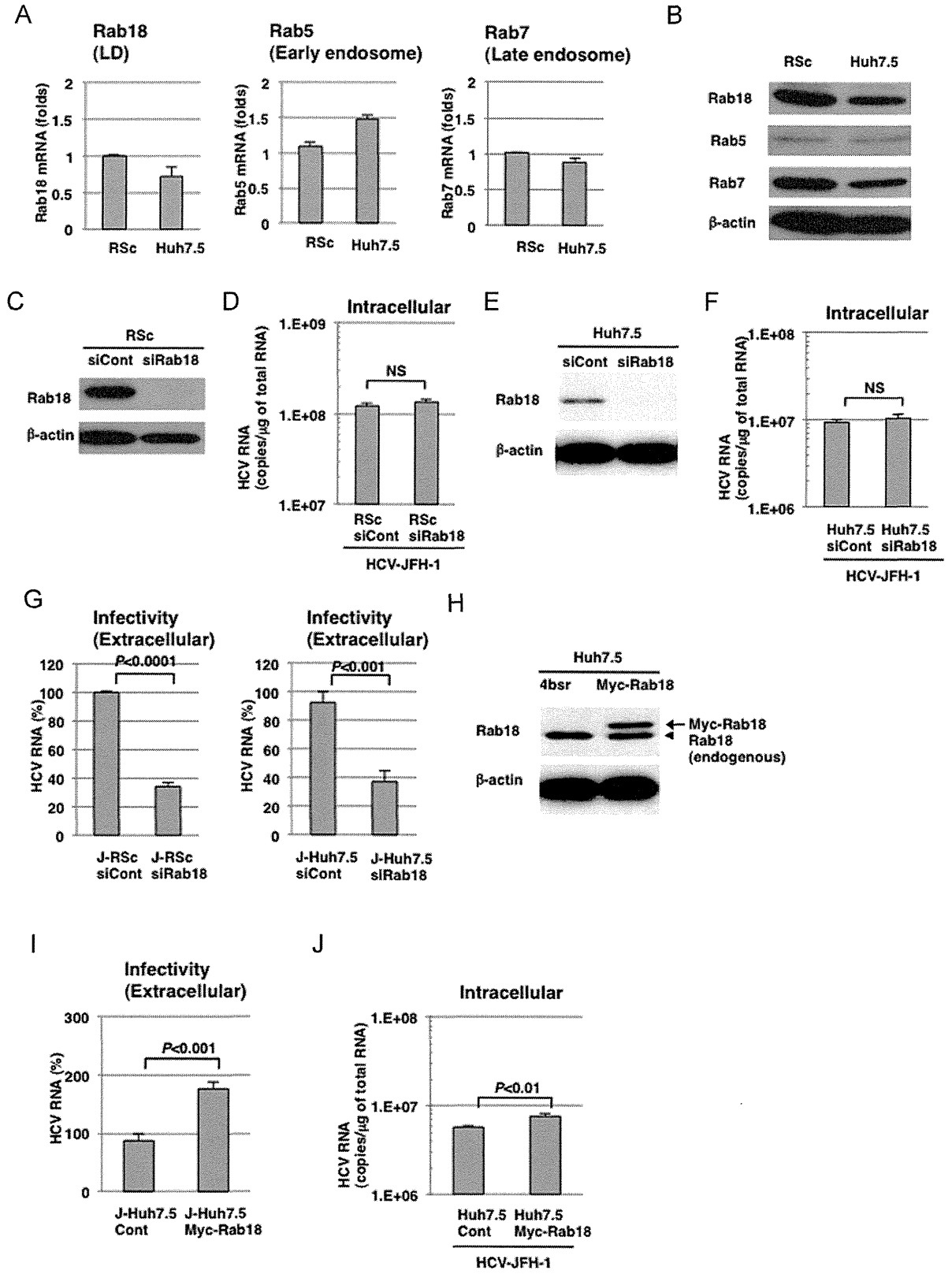

Fig. 2. Rab18 is required for viral production, but not viral RNA replication. (A) Quantitative RT-PCR analysis of Rab18, Rab5, and Rab7 mRNA in RSc and Huh7.5 cells. These levels were calculated relative to the level in RSc cells, which was set at 1. (B) Western blot analysis of Rab18, Rab5, and Rab7 in RSc and Huh7.5 cells. β-actin was included as a loading control. (C) Western blot analysis of Rab18 expression in RSc cells transfected with Rab18-specific (designated RSc siRab18 in the figure) or control (designated RSc siCont) siRNA. Cell lysates were prepared from RSc cells 120 h after transfection with Rab18-specific or control siRNA. (D) Quantitative RT-PCR analysis of HCV RNA in RSc siRab18 cells 24 h after infection with HCV-JFH-1. Transfection was performed 96 h before infection with HCV-JFH-1. NS: no significance. (E) Western blot analysis of Rab18 expression in Huh7.5 cells transfected with Rab18-specific (designated Huh7.5 siRab18) or control (designated Huh7.5 siCont) siRNA. (F) Quantitative RT-PCR analysis of HCV RNA in Huh7.5 siRab18 and siCont cells 24 h after infection with HCV-JFH-1. (G) Quantitative RT-PCR analysis of HCV RNA in Huh7.5 cells 72 h after infection with extracellular HCV-JFH-1. (Left panel) As extracellular HCV-JFH-1, the supernatant was recovered from RSc siCont cells (designated J-RSc siCont) or RSc siRab18 cells (designated J-RSc siRab18) 24 h after infection with HCV-JFH-1. (Right panel) The supernatant was also recovered from Huh7.5 siRab18 cells (designated J-Huh7.5 siRab18) and Huh7.5 siCont cells (designated J-Huh7.5 siCont) 24 h after infection with HCV-JFH-1. (H) Western blot analysis of Rab18 expression in Huh7.5 cells stably expressing Myc-tagged Rab18 (designated Huh7.5 Myc-Rab18). The arrow and arrowhead indicate exogenous (Myc-tagged) and endogenous Rab18, respectively. (I) Quantitative RT-PCR analysis of HCV RNA in Huh7.5 cells 72 h after infection with extracellular HCV-JFH-1. As extracellular HCV-JFH-1, the supernatant was recovered from Huh7.5 Cont (designated J-Huh7.5 Cont) or Huh7.5 Myc-Rab18 (designated J-Huh7.5 Myc-Rab18) 24 h after infection with HCV-JFH-1. (J) Quantitative RT-PCR analysis of HCV RNA in Huh7.5 Myc-Rab18 cells 24 h after infection with HCV-JFH-1.

genome-length HCV RNA (genotype 1b)-replicating cells (Mannova et al., 2006). These results may suggest that Rab18 also remained at the detergent-resistant membranes and the lipid rafts in the genome-length HCV RNA (genotype 1b)-replicating cells such as O cells. In addition, the gene silencing of Rab18 (Rab18-knockdown JFH-1-infected RSc cells) blocked localization of the HCV-JFH-1 core protein to LDs (Fig. 3D). Interestingly, the morphology of the population of HCV-JFH-1 core proteins was changed from a ring-like pattern to a dot-like pattern by the gene silencing of Rab18 (Fig. 3D). The HCV replication complex is formed on detergent-resistant membranes of the ER lumen (Shi et al., 2003). The ectopic expression of Rab18 induces the close apposition of LD to ER membranes through the reduction of ADRP (Ozeki et al., 2005). Rab18 may be one of the key host factors for the switch from the viral replication step to the viral assembly step through the close apposition of the detergent-resistant membranes to LDs. Rab18 may be an important target for the development of more effective anti-HCV reagents.

Materials and methods

Cell culture, reagents, and plasmids

Human hepatoma Huh7.5 cells were provided by Apath LLC (Brooklyn, NY). Huh7.5 cells, HuH-7 cells, and our established HuH-7-derived cells (sOC, Oc, OR6c, and RSc cells) were cultured in Dulbecco's modified Eagle's medium (Invitrogen, Carlsbad, CA) supplemented with 10% fetal bovine serum. Blasticidin (2 μg/ml) was used for the selection of Huh7.5 cells exogenously expressing Myc-Rab18. G418 (0.3 mg/ml) was also used for the selection of genome-length HCV RNA-replicating O cells.

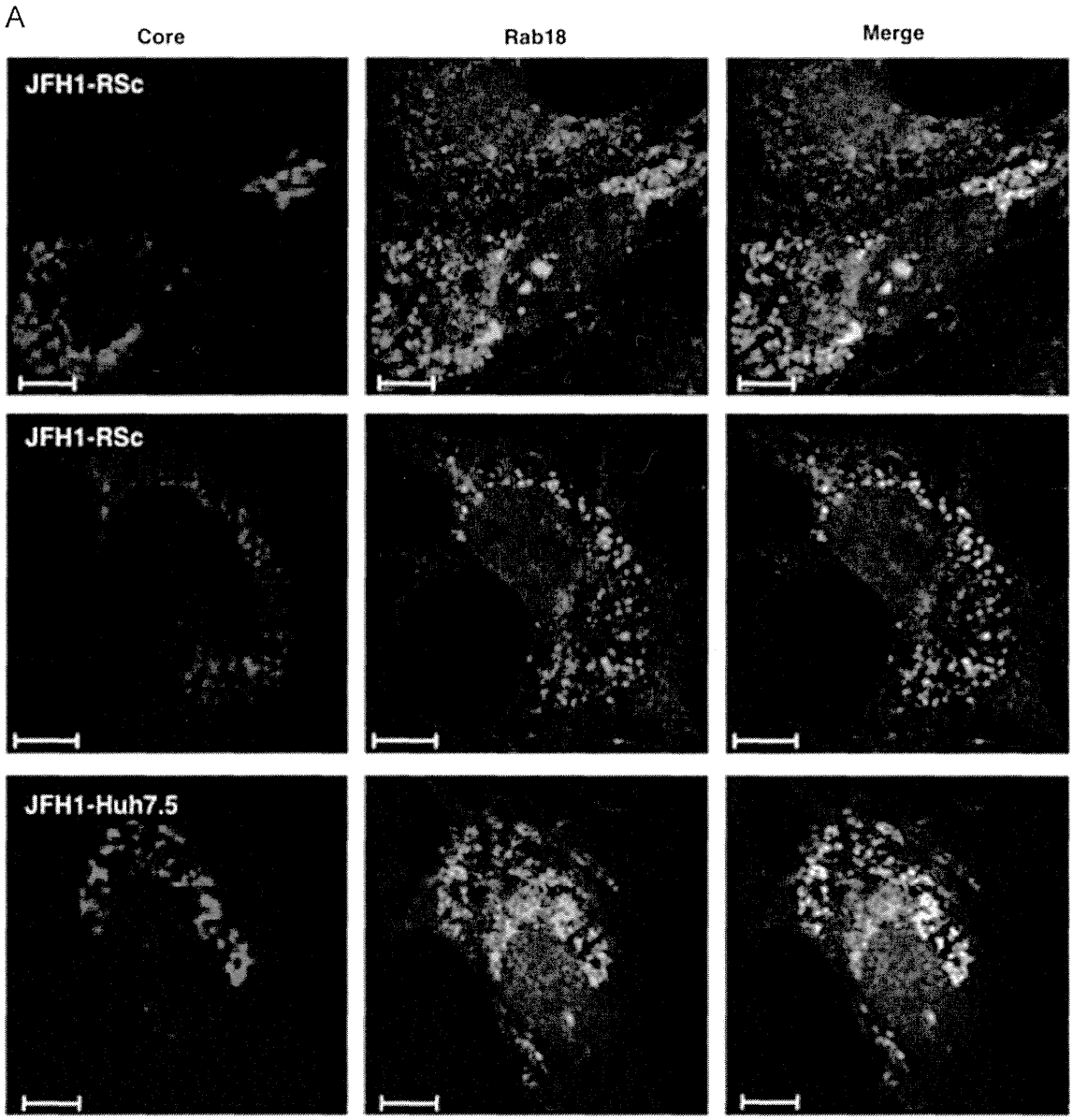

Fig. 3. Rab18 is required for viral assembly through the trafficking of HCV-JFH-1 core protein on LDs. (A) Visualization of the HCV-JFH-1 core protein (red) and Rab18 (green) under a confocal microscope. The panels show RSc or Huh7.5 cells 72 h after infection with HCV-JFH-1. Bars, 10 μm. (B) Visualization of the core protein (red) and Rab18 (green) in O cells. Bars, 10 μm. (C) Quantitative RT-PCR analysis of HCV RNA in Huh7.5 cells 72 h after infection with intracellular HCV-JFH-1. As intracellular HCV-JFH-1, the lysate was prepared from RSc siRab18 cells (designated J-RSc siRab18) and RSc siCont cells (designated J-RSc siCont) 24 h after infection with HCV-JFH-1. (D) Visualization of the HCV-JFH-1 core protein (red) and LD (green) under a confocal microscope. The panels show RSc siRab18 and siCont cells 72 h after infection with HCV-JFH-1. Bars, 10 μm.

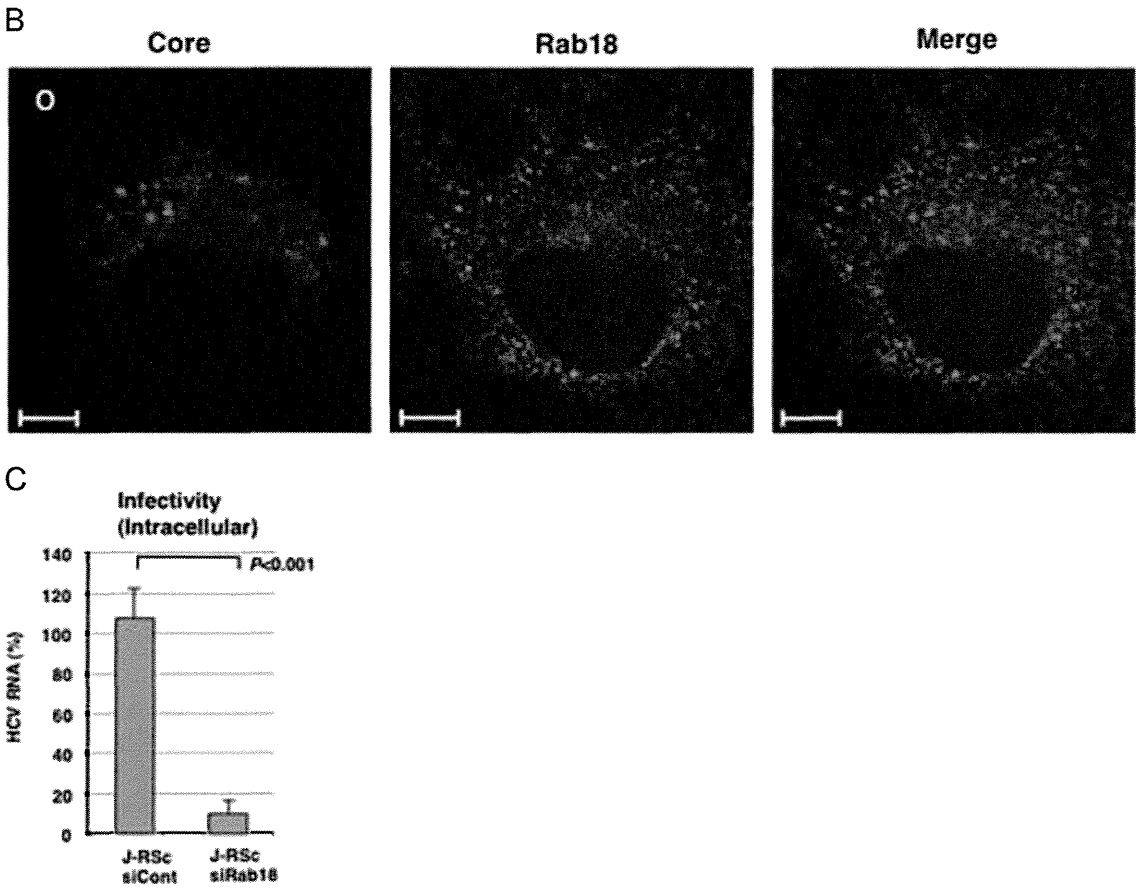

Fig. 3. (*continued*)

Immunofluorescence analysis

The LDs were stained with BODIPY493/503 (Invitrogen), and then photographed under a confocal microscope. Anti-Core antibody (CP11; Institute of Immunology, Tokyo, Japan) and anti-Rab18 antibody (Sigma, St. Louis, MO) were used as the primary antibodies. AlexaFluor 488-conjugated goat anti-rabbit antibody and AlexaFluor 594-conjugated goat anti-mouse antibody (Invitrogen) were used as the secondary antibodies. The intracellular localizations of HCV core protein and Rab18 were visualized and photographed under a confocal microscope as previously reported (Dansako et al., 2008). 4′-6-diamino-2-phenylindole (DAPI; Sigma) was used for visualization of the nucleus.

Flow cytometric analysis

The LDs were stained with BODIPY493/503 and then their mean fluorescence intensity was measured by a flow cytometer. The levels of LDs were calculated relative to the level in HuH-7 cells, which was set at 1.

Infection with HCV-JFH-1

The cells were infected with HCV-JFH1 (genotype 2a) for the appropriate time at a multiplicity of infection (MOI) of 1, and then the samples were prepared for the Western blot analysis, immunofluorescence analysis, and quantitative reverse transcription (RT)-PCR. Cell lysates and supernatants were prepared from the HCV-JFH-1-infected cells to monitor intracellular and extracellular infectivity. Intracellular HCV-JFH-1 was prepared from HCV-JFH-1-infected cells by repeated freeze-thaw cycles.

Generation of Rab18-knockdown cells

Small interfering RNAs (siRNAs) targeting Rab18 (Thermo Scientific; M-010824-00-0005) were prepared to generate Rab18-knockdown cells. siRNAs targeting Rab18 or non-targeting siRNAs (Thermo Scientific; D-001206-13-20) were introduced into RSc or Huh7.5 cells by DharmaFECT transfection reagent (Thermo Fisher Scientific, Waltham, MA). After transfection for the appropriate amount of time, Rab18-knockdown cells were infected with HCV-JFH-1.

Quantitative RT-PCR analysis

Total cellular RNA was isolated from HCV-JFH-1-infected cells by using an RNeasy mini kit (Qiagen, Hilden, Germany). RT was performed as previously described (Dansako et al., 2009). A SYBR Premix Ex Taq kit (TaKaRa Bio, Otsu, Japan) was used to measure the RNA levels of Rab18, Rab5, Rab7, GAPDH, or HCV. We used the following forward and reverse primer sets for quantitative PCR: for Rab18, 5′-GCGGAACGGGGTCAGGATGG-3′ (forward) and 5′-AAGAG CAGGCTGGACTTGCCC-3′ (reverse); for Rab5, 5′-GCTTGCTGCGGTCT CAGGTTTCT-3′ (forward) and 5′-TGGCCCGTTGGGTCTTGTTGC-3′ (reverse); for Rab7, 5′-CTCATCCAGGCCAGTCCCCGA-3′ (forward) and 5′–CCCGCTTTGTGGCCACTTGTC-3′ (reverse); for HCV and GAPDH, the primer sets are given in Dansako et al., 2013 and Dansako et al., 2003, respectively. The levels of Rab18, Rab5, Rab7, and HCV were normalized to the levels of GAPDH mRNA. The mRNA levels of Rab18, Rab5, and Rab7 in Huh7.5 cells were calculated relative to the level in RSc cells, which was set at 1. In vitro-transcribed HCV-JFH-1 RNA was used as the standard to calculate the amount of HCV RNA in HCV-JFH-1-infected cells. Data are the means ± SD from three independent experiments.

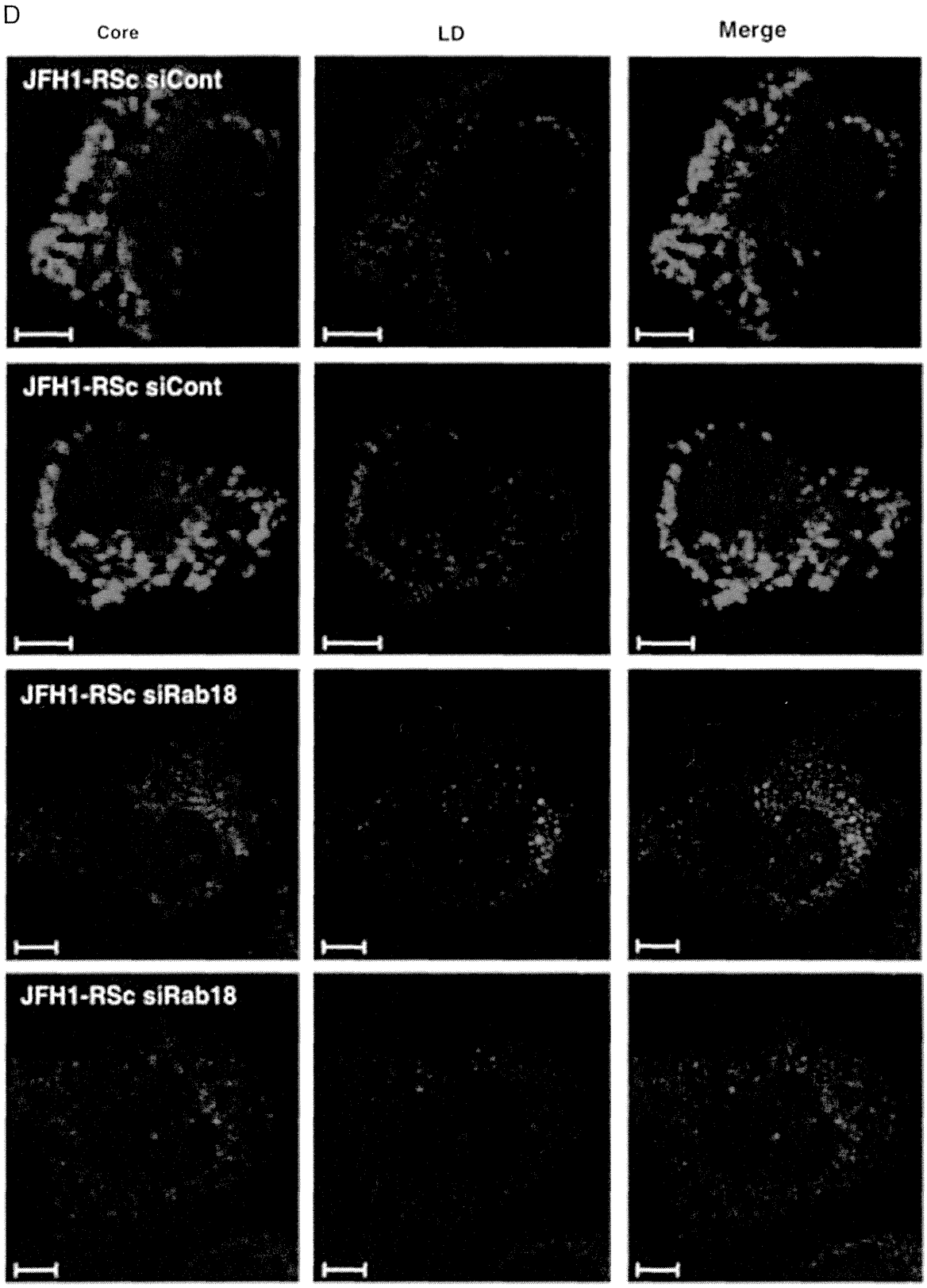

Fig. 3. (*continued*)

Western blot analysis

Preparation of cell lysates, and SDS-polyacrylamide gel electrophoresis were performed as previously described (Dansako et al., 2005). Gel was transferred to an Immobilon PVDF membrane (Millipore, Billerica, MA) by using a semi-dry transfer system: Horize BLOT 2MR (ATTO, Tokyo, Japan). Anti-Core (CP11; Institute of Immunology Co.), anti-Myc (PL14; Medical & Biological Laboratories, Nagoya, Japan), anti-Rab18 (Sigma), anti-Rab5 (S-19; Santa Cruz Biotechnology. Santa Cruz, CA), anti-Rab7 (Sigma),

and anti-β-actin antibody (AC-15; Sigma) were used in this study as primary antibodies. HRP-conjugated anti-mouse-IgG or anti-rabbit-IgG was used in this study as a secondary antibody (Cell Signaling Technology, Beverly, MA). Immunocomplexes were detected as previously described (Dansako et al., 2007).

Statistical analysis

Determination of the significance of differences among groups was assessed using the Student's *t*-test. $P < 0.05$ was considered statistically significant.

Acknowledgments

We thank Marie Iwado, Yoshiko Ueeda, Narumi Yamane and Takashi Nakamura for their technical assistance. We also thank Dr. Shinya Satoh for his helpful suggestions. This work was supported by Grants-in-Aid for Research on Hepatitis from the Ministry of Health, Labor, and Welfare of Japan; and by Japan Society for the Promotion of Science (JSPS) KAKENHI Grant no. 25293110.

Appendix A. Supplementary information

Supplementary data associated with this article can be found in the online version at http://dx.doi.org/10.1016/j.virol.2014.05.017.

References

Abe, K., Ikeda, M., Dansako, H., Naka, K., Kato, N., 2007. Cell culture-adaptive NS3 mutations required for the robust replication of genome-length hepatitis C virus RNA. Virus Res. 125, 88–97.

Ariumi, Y., Kuroki, M., Abe, K., Dansako, H., Ikeda, M., Wakita, T., Kato, N., 2007. DDX3 DEAD-box RNA helicase is required for hepatitis C virus RNA replication. J. Virol. 81, 13922–13926.

Ariumi, Y., Kuroki, M., Dansako, H., Abe, K., Ikeda, M., Wakita, T., Kato, N., 2008. The DNA damage sensors ataxia-telangiectasia mutated kinase and checkpoint kinase 2 are required for hepatitis C virus RNA replication. J. Virol. 82, 9639–9646.

Blight, K.J., McKeating, J.A., Rice, C.M., 2002. Highly permissive cell lines for subgenomic and genomic hepatitis C virus RNA replication. J. Virol. 76, 13001–13014.

Boulant, S., Douglas, M.W., Moody, L., Budkowska, A., Targett-Adams, P., McLauchlan, J., 2008. Hepatitis C virus core protein induces lipid droplet redistribution in a microtubule- and dynein-dependent manner. Traffic 9, 1268–1282.

Brasaemle, D.L., Dolios, G., Shapiro, L., Wang, R., 2004. Proteomic analysis of proteins associated with lipid droplets of basal and lipolytically stimulated 3T3-L1 adipocytes. J. Biol. Chem. 279, 46835–46842.

Choo, Q.L., Kuo, G., Weiner, A.J., Overby, L.R., Bradley, D.W., Houghton, M., 1989. Isolation of a cDNA clone derived from a blood-borne non-A, non-B viral-hepatitis genome. Science 244, 359–362.

Counihan, N.A., Rawlinson, S.M., Lindenbach, B.D., 2011. Trafficking of hepatitis C virus core protein during virus particle assembly. PLoS Pathog. 7, e1002302.

Dansako, H., Ikeda, M., Abe, K., Mori, K., Takemoto, K., Ariumi, Y., Kato, N., 2008. A new living cell-based assay system for monitoring genome-length hepatitis C virus RNA replication. Virus Res. 137, 72–79.

Dansako, H., Ikeda, M., Ariumi, Y., Wakita, T., Kato, N., 2009. Double-stranded RNA-induced interferon-beta and inflammatory cytokine production modulated by hepatitis C virus serine proteases derived from patients with hepatic diseases. Arch. Virol. 154, 801–810.

Dansako, H., Ikeda, M., Kato, N., 2007. Limited suppression of the interferon-beta production by hepatitis C virus serine protease in cultured human hepatocytes. FEBS J. 274, 4161–4176.

Dansako, H., Naganuma, A., Nakamura, T., Ikeda, F., Nozaki, A., Kato, N., 2003. Differential activation of interferon-inducible genes by hepatitis C virus core protein mediated by the interferon stimulated response element. Virus Res. 97, 17–30.

Dansako, H., Naka, K., Ikeda, M., Kato, N., 2005. Hepatitis C virus proteins exhibit conflicting effects on the interferon system in human hepatocyte cells. Biochem. Biophys. Res. Commun. 336, 458–468.

Dansako, H., Yamane, D., Welsch, C., McGivern, D.R., Hu, F.Y., Kato, N., Lemon, S.M., 2013. Class A scavenger receptor 1 (MSR1) restricts hepatitis C virus replication by mediating Toll-like receptor 3 recognition of viral RNAs produced in neighboring cells. PLoS Pathog. 9, e1003345.

Dejgaard, S.Y., Murshid, A., Erman, A., Kizilay, O., Verbich, D., Lodge, R., Dejgaard, K., Ly-Hartig, T.B., Pepperkok, R., Simpson, J.C., Presley, J.F., 2008. Rab18 and Rab43 have key roles in ER-Golgi trafficking. J. Cell Sci. 121, 2768–2781.

Hickenbottom, S.J., Kimmel, A.R., Londos, C., Hurley, J.H., 2004. Structure of a lipid droplet protein: the PAT family member TIP47. Structure 12, 1199–1207.

Hope, R.G., Murphy, D.J., McLauchlan, J., 2002. The domains required to direct core proteins of hepatitis C virus and GB virus-B to lipid droplets share common features with plant oleosin proteins. J. Biol. Chem. 277, 4261–4270.

Hutagalung, A.H., Novick, P.J., 2011. Role of Rab GTPases in membrane traffic and cell physiology. Physiol. Rev. 91, 119–149.

Ikeda, M., Abe, K., Dansako, H., Nakamura, T., Naka, K., Kato, N., 2005. Efficient replication of a full-length hepatitis C virus genome, strain O, in cell culture, and development of a luciferase reporter system. Biochem. Biophys. Res. Commun. 329, 1350–1359.

Ikeda, M., Abe, K., Yamada, M., Dansako, H., Naka, K., Kato, N., 2006. Different anti-HCV profiles of statins and their potential for combination therapy with interferon. Hepatology 44, 117–125.

Kato, N., 2001. Molecular virology of hepatitis C virus. Acta Med. Okayama 55, 133–159.

Kato, N., Mori, K., Abe, K., Dansako, H., Kuroki, M., Ariumi, Y., Wakita, T., Ikeda, M., 2009. Efficient replication systems for hepatitis C virus using a new human hepatoma cell line. Virus Res. 146, 41–50.

Kato, N., Sugiyama, K., Namba, K., Dansako, H., Nakamura, T., Takami, M., Naka, K., Nozaki, A., Shimotohno, K., 2003. Establishment of a hepatitis C virus subgenomic replicon derived from human hepatocytes infected in vitro. Biochem. Biophys. Res. Commun. 306, 756–766.

Kenworthy, R., Lambert, D., Yang, F., Wang, N., Chen, Z., Zhu, Haizhen, Zhu, F., Liu, C., Li, K., Tang, H., 2009. Short-hairpin RNAs delivered by lentiviral vector transduction trigger RIG-I-mediated IFN activation. Nucleic Acids Res. 37, 6587–6599.

Mannova, P., Fang, R.H., Wang, H., Deng, B., McIntosh, M.W., Hanash, S.M., Beretta, L., 2006. Modification of host lipid raft proteome upon hepatitis C virus replication. Mol. Cell. Proteomics 5, 2319–2325.

Matto, M., Rice, C.M., Aroeti, B., Glenn, J.S., 2004. Hepatitis C virus core protein associates with detergent-resistant membranes distinct from classical plasma membrane rafts. J. Virol. 78, 12047–12053.

Miyanari, Y., Atsuzawa, K., Usuda, N., Watashi, K., Hishiki, T., Zayas, M., Bartenschlager, R., Wakita, T., Hijikata, M., Shimotohno, K., 2007. The lipid droplet is an important organelle for hepatitis C virus production. Nat. Cell Biol. 9, 1089–1097.

Ohkoshi, S., Kojima, H., Tawaraya, H., Miyajima, T., Kamimura, T., Asakura, H., Satoh, A., Hirose, S., Hijikata, M., Kato, N., Shimotohno, K., 1990. Prevalence of antibody against non-A, non-B hepatitis-virus in Japanese patients with hepatocellular-carcinoma. Jpn. J. Cancer Res. 81, 550–553.

Ohsaki, Y., Maeda, T., Maeda, M., Tauchi-Sato, K., Fujimoto, T., 2006. Recruitment of TIP47 to lipid droplets is controlled by the putative hydrophobic cleft. Biochem. Biophys. Res. Commun. 347, 279–287.

Ozeki, S., Cheng, J.L., Tauchi-Sato, K., Hatano, N., Taniguchi, H., Fujimoto, T., 2005. Rab18 localizes to lipid droplets and induces their close apposition to the endoplasmic reticulum-derived membrane. J. Cell Sci. 118, 2601–2611.

Salloum, S., Wang, H., Ferguson, C., Parton, R.G., Tai, A.W., 2013. Rab18 binds to hepatitis C virus NS5A and promotes interaction between sites of viral replication and lipid droplets. PLoS Pathog. 9, e1003513.

Shavinskaya, A., Boulant, S., Penin, F., McLauchlan, J., Bartenschlager, R., 2007. The lipid droplet binding domain of hepatitis C virus core protein is a major determinant for efficient virus assembly. J. Biol. Chem. 282, 37158–37169.

Shi, S.T., Lee, K.J., Aizaki, H., Hwang, S.B., Lai, M.M.C., 2003. Hepatitis C virus RNA replication occurs on a detergent-resistant membrane that cofractionates with caveolin-2. J. Virol. 77, 4160–4168.

Targett-Adams, P., Boulant, S., McLauchlan, J., 2008. Visualization of double-stranded RNA in cells supporting hepatitis C virus RNA replication. J. Virol. 82, 2182–2195.

The American Journal of Pathology, Vol. 184, No. 11, November 2014

ELSEVIER

The American Journal of
PATHOLOGY

ajp.amjpathol.org

GASTROINTESTINAL, HEPATOBILIARY, AND PANCREATIC PATHOLOGY

Hepatitis C Virus Core Protein Suppresses Mitophagy by Interacting with Parkin in the Context of Mitochondrial Depolarization

Yuichi Hara,* Izumi Yanatori,† Masanori Ikeda,‡ Emi Kiyokage,§ Sohji Nishina,* Yasuyuki Tomiyama,* Kazunori Toida,§ Fumio Kishi,† Nobuyuki Kato,‡ Michio Imamura,¶ Kazuaki Chayama,¶ and Keisuke Hino*

From the Departments of Hepatology and Pancreatology, Molecular Genetics,† and Anatomy,§ Kawasaki Medical School, Kurashiki; the Department of Tumor Virology,‡ Okayama University Graduate School of Medicine, Dentistry and Pharmaceutical Sciences, Okayama; and the Department of Gastroenterology and Metabolism,¶ Applied Life Sciences, Institute of Biomedical and Health Sciences, Hiroshima University, Hiroshima, Japan*

Accepted for publication July 25, 2014.

Address correspondence to Keisuke Hino, M.D., Ph.D., Department of Hepatology and Pancreatology, Kawasaki Medical School, 577 Matsushima, Kurashiki, Okayama 701-0192, Japan. E-mail: khino@med.kawasaki-m.ac.jp.

Hepatitis C virus (HCV) causes mitochondrial injury and oxidative stress, and impaired mitochondria are selectively eliminated through autophagy-dependent degradation (mitophagy). We investigated whether HCV affects mitophagy in terms of mitochondrial quality control. The effect of HCV on mitophagy was examined using HCV-Japanese fulminant hepatitis-1–infected cells and the uncoupling reagent carbonyl cyanide *m*-chlorophenylhydrazone as a mitophagy inducer. In addition, liver cells from transgenic mice expressing the HCV polyprotein and human hepatocyte chimeric mice were examined for mitophagy. Translocation of the E3 ubiquitin ligase Parkin to the mitochondria was impaired without a reduction of pentaerythritol tetranitrate–induced kinase 1 activity in the presence of HCV infection both *in vitro* and *in vivo*. Coimmunoprecipitation assays revealed that Parkin associated with the HCV core protein. Furthermore, a Yeast Two-Hybrid assay identified a specific interaction between the HCV core protein and an N-terminal Parkin fragment. Silencing Parkin suppressed HCV core protein expression, suggesting a functional role for the interaction between the HCV core protein and Parkin in HCV propagation. The suppressed Parkin translocation to the mitochondria inhibited mitochondrial ubiquitination, decreased the number of mitochondria sequestered in isolation membranes, and reduced autophagic degradation activity. Through a direct interaction with Parkin, the HCV core protein suppressed mitophagy by inhibiting Parkin translocation to the mitochondria. This inhibition may amplify and sustain HCV-induced mitochondrial injury. *(Am J Pathol 2014, 184: 3026–3039; http://dx.doi.org/10.1016/j.ajpath.2014.07.024)*

Oxidative stress is present in chronic hepatitis C to a greater degree than in other inflammatory liver diseases.[1,2] The hepatitis C virus (HCV) core protein induces the production of reactive oxygen species (ROS)[3,4] through mitochondrial electron transport inhibition.[5] Because the mitochondria are targets for ROS and ROS generators, HCV-induced ROS have the potential to injure mitochondria. In addition, hepatocellular mitochondrial alterations have been observed in patients with chronic hepatitis C.[6] We previously identified a ROS-associated iron metabolic disorder[7] and demonstrated that transgenic mice expressing the HCV polyprotein develop hepatocarcinogenesis related to mitochondrial injury induced by HCV and iron overload.[8] Therefore, impaired mitochondrial function may play a critical role in the development of hepatocellular carcinoma (HCC) in patients with chronic HCV infection. Conversely, the affected mitochondria are selectively eliminated through the autophagy-dependent degradation of mitochondria (referred to as mitophagy) in both physiological and pathological settings to maintain the mitochondrial quality.[9,10] On the

Supported by Japan Society for the Promotion of Science Grant-in-Aid for Scientific Research (B) 23390201 and Grant-in-Aid for Exploratory Research 25670374; Ministry of Health, Labor and Welfare of Japan Health and Labor Sciences Research grant 25200601 for research on hepatitis; and Kawasaki Medical School Research Project grant P2.

Disclosures: None declared.

Current address of M.I., Kagoshima University Graduate School of Medical and Dental Sciences, Kagoshima, Japan.

http://dx.doi.org/10.1016/j.ajpath.2014.07.024

basis of these observations, we hypothesized that HCV may suppress mitophagy, which could lead to the sustained presence of affected mitochondria, increased ROS production, and the development of HCC.

Mitochondrial membrane depolarization precedes mitophagy induction,[11] which is selectively controlled by a variety of proteins in mammalian cells, including pentaerythritol tetranitrate–induced kinase 1 (PINK1) and the E3 ubiquitin ligase Parkin.[12–19] PINK1 facilitates Parkin targeting of the depolarized mitochondria.[12–15] Although Parkin ubiquitinates a broad range of mitochondrial outer membrane proteins,[14,17–19] it remains unclear how Parkin enables the damaged mitochondria to be recognized by the autophagosome. Structures containing autophagy-related protein 9A and the uncoordinated family member-51–like kinase 1 complex independently target depolarized mitochondria at the initial stages of Parkin-mediated mitophagy, whereas the autophagosomal microtubule-associated protein light chain 3 (LC3) is critical for efficient incorporation of damaged mitochondria into the autophagosome at a later stage.[20] LC3-I undergoes post-translational modification by phosphatidylethanolamine to become LC3-II, and LC3-II insertion into the autophagosomal membrane is a key step in autophagosome formation. In addition, the autophagic adaptor p62 is recruited to mitochondrial clusters and is essential for mitochondrial clearance,[13] although it remains controversial as to whether p62 is essential for mitochondrial recognition by the autophagosome[13] or rather is important for perinuclear clustering of depolarized mitochondria.[19,21] Our aim was to examine whether HCV suppresses mitophagy. We found that HCV core protein inhibits the translocation of Parkin to affected mitochondria by interacting with Parkin and subsequently suppressing mitophagy. These results imply that mitochondria affected by HCV core protein are unlikely to be eliminated, which may intensify oxidative stress and increase the risk of hepatocarcinogenesis.

Materials and Methods

Cell Culture, HCV Infection Experiments, and Mitochondrial Depolarization

HCV-Japanese fulminant hepatitis-1 (JFH1)–infected Huh7 cells have previously been described in detail.[22] The supernatants were collected from cell culture–generated JFH1-Huh7 cells at 21 days after infection and stored until use at −80°C after filtering through a 0.45-μm filter. For infection experiments with the HCV-JFH1 virus, 1×10^5 Huh7 cells per well were plated onto 6-well plates and cultured for 24 hours. Then, we infected the cells with 50 μL (equivalent to a multiplicity of infection of 0.1) of inoculum. The culture supernatants were collected, and the levels of the HCV core were determined using an enzyme-linked immunosorbent assay (ELISA; Mitsubishi Kagaku Bio-Clinical Laboratories, Tokyo, Japan). Total RNA was isolated from the infected cellular lysates using an RNeasy mini kit (Qiagen, Hilden, Germany) for quantitative RT-PCR analysis of the intracellular HCV RNA. The HCV infectivity in the culture supernatants was determined by a focus-forming assay at 48 hours after infection. The HCV-infected cells were detected using an anti-HCV core antibody (CP-9 and CP-11, Institute of Immunology, Ltd, Tokyo, Japan). Intracellular HCV infectivity was determined using a focus-forming assay at 48 hours after inoculation of the lysates by repeated freeze-and-thaw cycles (three times).

To depolarize the mitochondria, the cells were treated with 10 μmol/L carbonyl cyanide *m*-chlorophenylhydrazone (CCCP; Sigma-Aldrich, St. Louis, MO) for 1 to 2 hours or 1 μmol/L valinomycin (Sigma-Aldrich) for 3 hours; CCCP represses ATP synthesis through the loss of the H^+ gradient without affecting mitochondrial electron transport, which is known to induce mitochondrial fragmentation.[13]

Animals

The pAlbSVPA-HCV vector, which contains the full-length polyprotein-coding region under the control of the murine albumin promoter/enhancer, has previously been described in detail.[23,24] Of the four transgenic lineages with evidence of RNA transcription of the full-length HCV-N open reading frame (FL-N), the FL-N/35 lineage proved capable of breeding large numbers.[24] Urokinase-type plasminogen activator–transgenic severe combined immunodeficiency mice were generated, and human hepatocytes were transplanted to generate chimeric mice.[25] The chimeric mice were injected with genotype *1b* HCV-positive human serum samples, as described previously.[26] The mouse livers were extracted 12 weeks after the infection, when the serum HCV RNA titers had increased over baseline levels. Male FL-N/35 transgenic mice, age-matched C57BL/6 mice (control), and chimeric mice with and without HCV infection were fed, maintained, and then euthanized by i.p. injection of 10% nembutal sodium, according to the guidelines approved by the Institutional Animal Care and Use Committee. The study protocol for obtaining human serum samples conformed to the ethical guidelines of the 1975 Declaration of Helsinki and was approved by the Institutional Review Committee.

Measurement of HCV RNA and Human Albumin in the Serum of Chimeric Mice

HCV RNA[26] and human albumin[25] were quantified as described previously. Human albumin levels in the serum of chimeric mice were determined using the Human Albumin ELISA Quantification kit (Bethyl Laboratories Inc., Montgomery, TX).

Measurement of Mitochondrial Membrane Potential

The mitochondrial membrane potential ($\Delta\Psi$) was measured using a Cell Meter JC-10 Mitochondrial Membrane Potential Assay kit (AAT Bioquest, Inc., Sunnyvale, CA), according to the manufacturer's instructions. The fluorescent intensities

for both J-aggregates (red) and monometric forms (green) of JC-10 were measured at Ex/Em = 490/525 nm and 540/590 nm with a Varioskan Flush Multimode Reader (Thermo Fisher Scientific, Waltham, MA).

Isolation of Mitochondria

The cells were lysed by mechanical homogenization using a small pestle, and mitochondrial extraction was performed using a Qproteome Mitochondria Isolation kit (Qiagen), according to the manufacturer's instructions. Liver mitochondria were isolated as described previously with some modifications.[27] In brief, the livers were minced on ice and homogenized by five strokes with a Dounce homogenizer and a tight-fitting pestle in isolation buffer [70 mmol/L sucrose, 1 mmol/L KH_2PO_4, 5 mmol/L HEPES, 220 mmol/L mannitol, 5 mmol/L sodium succinate, and 0.1% bovine serum albumin (BSA), pH 7.4]. The homogenate was centrifuged at 800 × *g* for 5 minutes at 4°C. The supernatant fraction was retained, whereas the pellet was washed with isolation buffer and centrifuged again. The combined supernatant fractions were centrifuged at 1000 × *g* for 15 minutes at 4°C to obtain a crude mitochondrial pellet.

Measurement of ROS

The cellular ROS level was measured by oxidation of the cell-permeable, oxidation-sensitive fluorogenic precursor, *2′,7′*-dihydrodichlorofluorescein diacetate (Molecular Probes Inc., Eugene, OR). Fluorescence was measured using a Varioskan Flush Multimode Reader at 495/535 nm (excitation/emission).

Determination of Glutathione Content

Mitochondrial pellets were measured for total glutathione [reduced glutathione (GSH) + oxidized glutathione (GSSG)] and GSH content using the GSSG/GSH Quantification kit (Dojindo Molecular Technologies, Inc., Kumamoto, Japan). The concentration of GSH was calculated using the following formula:

$$\text{GSH concentration} = \text{Total glutathione concentration} - [\text{GSSG concentration}] \times 2 \quad (1)$$

The liver tissue samples (approximately 50 mg) were minced in ice-cold metaphosphoric acid solution, homogenized, and centrifuged at 3000 × *g* for 10 minutes at 4°C. Lysates from the liver tissue samples and mitochondrial samples (2 mg) were evaluated for the concentration of GSH using the thioester method and a GSH-400 kit (Oxis International Inc., Portland, OR) and for total glutathione content using the glutathione reductase–dinitrothiocyanobenzene recycling assay and the GSH-412 kit (Oxis International Inc.), as described previously.[5]

Immunoblotting

Samples were lysed in radioimmunoprecipitation assay buffer [20 mmol/L Tris-HCl (pH 7.5), 150 mmol/L NaCl, 50 mmol/L NaF, 1 mmol/L Na_3VO_4, 0.1% SDS, and 0.5% Triton X-100], as described previously,[28] supplemented with 1% protease inhibitor mixture (Sigma-Aldrich) and 100 mmol/L phenylmethylsulfonyl fluoride. Cell lysates or mitochondrial pellets were subjected to immunoblot analysis using an iBlot Gel Transfer Device (Invitrogen, Carlsbad, CA). The membranes were incubated with the following primary antibodies: rabbit anti-human LC3 (Novus Biologicals, Littleton, CO), rabbit anti-human p62/SQSTM1 (MBL, Nagoya, Japan), rabbit anti-human Parkin (Cell Signaling Technology, Danvers, MA), mouse anti-human Parkin (Santa Cruz Biotechnology, Inc.), rabbit anti-human p-Parkin (Ser 378; Santa Cruz Biotechnology, Inc.), rabbit anti-human PINK1 (Cell Signaling Technology), mouse anti-human mitochondrial heat shock protein-70 (BioReagents, Golden, CO), mouse anti-human ubiquitin (Santa Cruz Biotechnology, Inc.), goat anti-human voltage-dependent anion-selective channel protein 1 (VDAC1; Santa Cruz Biotechnology, Inc.), monoclonal antisynthetic HCV core peptide (CP11; Institute of Immunology, Ltd), mouse anti-HCV non-structural (NS) 3 protein (Abcam, Cambridge, MA), mouse anti-HCV NS4A (Abcam), mouse anti-HCV NS5A protein (Abcam), and rabbit anti-human β-actin (Cell Signaling Technology).

Electron Microscopy

To address the detail localization of core and Parkin, the cells treated with CCCP for 1 hour were fixed with 4% paraformaldehyde and 1% glutaraldehyde in 0.1 mol/L Millonig's phosphate buffer (pH 7.4) for 30 minutes. The cells were incubated with a mixture of the following primary antibodies in phosphate-buffered saline (PBS) containing 1% BSA and 0.05% sodium azide overnight at 20°C: mouse monoclonal antisynthetic HCV core peptide (Institute of Immunology), rabbit anti-human Parkin (Abcam), and rabbit anti-rat LC3 (Wako Pure Chemical Industries, Ltd, Osaka, Japan). After washing with PBS, the cells were incubated with biotinylated donkey anti-rabbit IgG (Jackson ImmunoResearch Laboratories, Inc., Baltimore Pike, PA) in 1% BSA for 2 hours at 20°C. After washing with PBS, the cells were incubated with Alexa Fluor-488 FluoroNanogold-streptavidin (Jackson ImmunoResearch Laboratories, Inc.), indocarbocyanine-labeled donkey anti-mouse IgG (Jackson ImmunoResearch Laboratories, Inc.), and indocarbocyanine-labeled donkey anti-rabbit IgG (Jackson ImmunoResearch Laboratories, Inc.) in 1% BSA for 2 hours at 20°C. After washing with PBS, the cells were incubated with mouse peroxidase–anti-peroxidase complex (Jackson ImmunoResearch Laboratories, Inc.) in PBS for 3 hours at 20°C. The peroxidase reduction was developed with 0.05% diaminobenzidine tetrahydrochloride in 50 mmol/L Tris buffer containing 0.01% hydrogen peroxide for 20 minutes at room temperature. The diameter of the gold immunoparticles was increased using a silver enhancement kit (HQ silver; Nanoprobes, Inc., Yaphank, NY) for 4 minutes at

room temperature. After treatment with 1% osmium and 2% uranyl acetate, the cells were dehydrated in a graded series of ethanol and embedded in Epon-Araldite (OKEN, Tokyo, Japan). Serial ultrathin sections (each 70 nm thick) were examined using an electron microscope (model JEM1400; JEOL, Tokyo, Japan). These immune–electron microscopic methods were generally performed according to our previous study.[29]

Immunofluorescence Microscopy

The cells were fixed, permeabilized, and immunostained with rabbit anti-human Parkin (Abcam), goat anti-human Parkin (Santa Cruz Biotechnology, Inc.), goat anti-human Tom20 (Santa Cruz Biotechnology, Inc.), rabbit anti-rat LC3 (Wako Pure Chemical Industries, Ltd), or mouse monoclonal anti-synthetic HCV core peptide (Institute of Immunology) antibodies, followed by Cy3-conjugated donkey anti-rabbit IgG (Jackson ImmunoResearch Laboratories, Inc.), fluorescein isothiocyanate–conjugated donkey anti-goat IgG (Jackson ImmunoResearch Laboratories, Inc.), or Alexa Fluor 647–conjugated donkey anti-mouse IgG (Jackson ImmunoResearch Laboratories, Inc.). Cell images were captured using a confocal microscope (model LSM700; Zeiss, Jena, Germany) equipped with 488-, 555-, and 639-nm diodes. The images were acquired in a sequential mode using a 63× Plan Apochromat numerical aperture/1.4 oil objective and the appropriate filter combinations. All images were saved as tagged image file format files. The contrast was adjusted using Photoshop version CS5 (Adobe, San Jose, CA), and the images were imported into Illustrator version CS5 (Adobe). Colocalization was assessed with line scans using ImageJ software version 1.46 (NIH, Bethesda, MD).

Coimmunoprecipitation

Coimmunoprecipitation was performed using a Dynabeads Co-Immunoprecipitation Kit (Invitrogen), according to the manufacturer's instructions. Magnetic beads (Dynabeads M-270 Epoxy) were conjugated to anti-VDAC1 (Santa Cruz Biotechnology, Inc.), anti-Parkin (Cell Signaling Technology), anti-ubiquitin (Santa Cruz Biotechnology, Inc.), or anti-p62 (MBL) antibodies by rotating overnight at 37°C. The antibody-Dynabeads complex was then treated with coupling buffer. Beads coupled to anti-VDAC, anti-Parkin, anti-ubiquitin, or anti-p62 were incubated with cell lysates for 30 minutes at 4°C and then washed with coupling buffer. Collected protein complexes were subjected to immunoblot analysis using anti-VDAC, anti-ubiquitin (Santa Cruz Biotechnology, Inc.), and anti-Parkin (Cell Signaling Technology) antibodies to detect coimmunoprecipitated VDAC1, ubiquitin, and Parkin. Immunoblots using anti-Parkin, anti-HCV core (Institute of Immunology), anti-HCV NS3 (Abcam), anti-HCV NS4A (Abcam), or anti-HCV NS5A (Abcam) antibodies were performed to detect the coimmunoprecipitation of Parkin with core, NS3, NS4A, or NS5A protein.

RNA Interference

The siRNA knockdown oligonucleotides were obtained from Invitrogen. JFH1-Huh7 cells and/or Huh7 cells were grown to 50% to 60% confluency and transfected with 100 pmol siRNA oligonucleotides [5′-GGACGCUGUUCCUCGUUAUGAA-GAA-3′ (forward) and 5′-UUCUUCAUAACGAGGAACA-GCGUCC-3′ (reverse)] for PINK1 or siRNA oligonucleotides [5′-UCCAGCUCAAGGAGGUGGUUGCUAA-3′ (forward) and 5′-UUAGCAACCACCUCCUUGAGCUGGA-3′ (reverse)] for Parkin using Lipofectamine 2000 (Invitrogen). The cells were analyzed 72 hours after transfection.

Yeast Two-Hybrid Assay

A Matchmaker Gal4 two-hybrid system 3 (Clontech Laboratories, Inc., Mountain View, CA) was used according to the manufacturer's instructions. *Saccharomyces cerevisiae* Y187, containing an N- or C-terminal fragment cDNA of Parkin as a prey cloned into the Gal4-activation domain vector (pACT2), was allowed to mate with *S. cerevisiae* AH109, which had been transformed with a Gal4 DNA-binding domain vector (pGBKT7) containing the HCV core as bait. In addition, *S. cerevisiae* Y187, with the HCV core as a prey cloned into the Gal4-activation domain vector (pACT2), was allowed to mate with *S. cerevisiae* AH109, which had been transformed with a Gal4 DNA-binding domain vector (pGBKT7) containing N- or C-terminal fragment cDNA of Parkin as bait. To construct the prey and the bait, two regions of the Parkin gene that encoded the N-terminal 215–amino acid residues (1 to 215) and the C-terminal 250–amino acid residues (216 to 465) were amplified using PCR with genomic cDNA, and the HCV core gene was amplified with the HCV-O (genotype *1b*) genomic cDNA.[30] The PCR primers were as follows with the incorporated BamHI and EcoRI sites underlined: Parkin 1 to 215, 5′-GGATCCGCATGATAGTGTTTGTCAGGTT-3′ (forward) and 5′-GAATTCCTAGTGTGCTCCACATTTAA-AGA-3′ (reverse); Parkin 216 to 465, 5′-GGATCCGCCC-CACCTCTGACAAGGAAAC-3′ (forward) and 5′-GAAT-TCCTACACGTCGAACCAGTGGT-3′ (reverse); and HCV core, 5′-GAATTCGCCATGAGCACAAATCCTAAACCT-C-3′ (forward) and 5′-GGATCCTTAAGCGGAAGCTGG-GATGGTCAAA-3′ (reverse).

Real-Time RT-PCR

Total RNA was extracted from frozen liver tissues and cells using the RNeasy mini kit (Qiagen). Total RNA (2 μg) was reverse transcribed to cDNA using the High-Capacity RNA to cDNA kit (Applied Biosystems, Foster City, CA), according to the manufacturer's instructions. TaqMan Gene Expression Assays for LC3B, glyceraldehyde-3-phosphate dehydrogenase (GAPDH), Parkin, and HCV core were purchased from Applied Biosystems, and mRNA levels were quantified in triplicate using an Applied Biosystems

7500 Real-Time PCR system, according to the supplier's recommendations. The expression value for LC3B, Parkin, and HCV core mRNA was normalized to that of GAPDH.

Statistical Analysis

Quantitative values are expressed as the means ± SD. Data were compared between the two groups using the Student's *t*-test. $P < 0.05$ was considered significant.

Results

Mitochondrial Oxidative Status *in Vitro* and *in Vivo*

After treatment with CCCP, a widely adopted reagent for inducing mitophagy, the mitochondrial membrane potential ($\Delta\Psi$) was significantly reduced irrespective of HCV infection (Figure 1A). The ratio of reduced/total glutathione content was decreased in the mitochondrial fraction after CCCP treatment in JFH1-Huh7 cells (Figure 1B). Thus, the mitochondrial oxidative status after CCCP treatment was present in HCV-infected cells (JFH1-Huh7). The ratio of reduced/total glutathione content was also decreased in the mitochondrial fraction but not in the whole liver in transgenic mice and HCV-infected chimeric mice compared with the control mice (Figure 1, C and D). These results suggest that there is a baseline oxidation level within the mitochondrial glutathione pool in these transgenic mice and HCV-infected chimeric mice. Furthermore, the mitochondria in these transgenic mice and HCV-infected chimeric mice can undergo mitophagy.

Impaired Recruitment of Parkin to the Mitochondria

Parkin phosphorylation and translocation to the mitochondria after CCCP treatment are indispensable for mitochondrial ubiquitination and subsequent autophagosome formation during the course of mitophagy.[13,15] CCCP exposure induced Parkin accumulation in the mitochondria of Huh7 cells; however, this Parkin recruitment seemed to be inhibited in JFH1-Huh7 cells (Figure 2A). CCCP treatment induces mitochondrial fission, followed by mitophagy.[13] CCCP-treated Huh7 cells displayed fragmented mitochondria colocalized with Parkin, except for a few mitochondrial tubular network cells. Western blot analysis also showed that CCCP-induced recruitment of Parkin to the mitochondria was suppressed without any change in Parkin expression or phosphorylation levels in whole cell lysates of JFH1-Huh7 cells (Figure 2B). Neither CCCP treatment nor HCV infection significantly increased the mRNA levels of Parkin in Huh7 cells, even though there was a tendency of increase in Parkin mRNA after HCV infection (Figure 2C). These results indicate that HCV infection could inhibit Parkin recruitment to CCCP-induced depolarized mitochondria.

The unique and high concentration of CCCP (10 μmol/L) used in the present study may have affected cellular functions

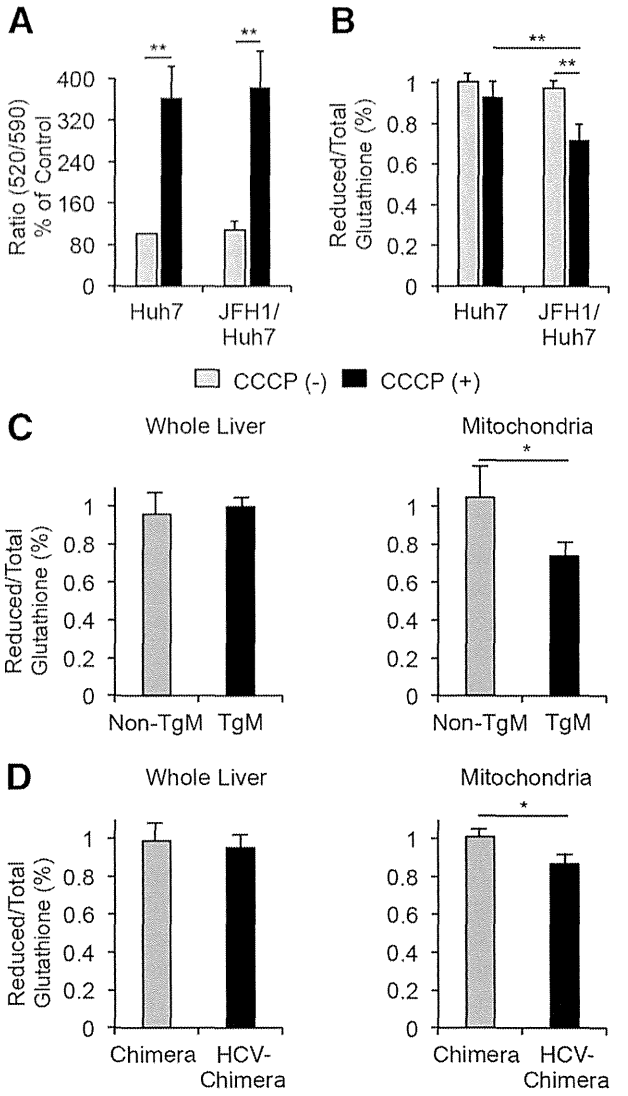

Figure 1 Mitochondrial membrane potential ($\Delta\Psi$) and glutathione content. **A:** Changes in $\Delta\Psi$ levels after a 1-hour carbonyl cyanide *m*-chlorophenylhydrazone (CCCP) treatment for Huh7 and JFH1-Huh7 cells ($n = 5$). The *y* axis represents the ratio of red (JC-10 aggregate form)/green (JC-10 monometric form) fluorescence intensity. **B:** Reduced and total glutathione content in mitochondrial fractions ($n = 5$). Reduced glutathione content was normalized to total glutathione content. Reduced and total glutathione content of freshly isolated whole liver homogenates or mitochondrial fractions of transgenic livers ($n = 7$, **C**) or HCV-infected chimeric mice livers ($n = 5$, **D**) compared with the content in the corresponding control liver samples. Reduced glutathione content was normalized to total glutathione content. $^*P < 0.05$, $^{**}P < 0.01$.

other than the proton gradient,[31] which suggests that Parkin translocation from the cytoplasm to the mitochondria may not be induced specifically through mitochondrial depolarization. Therefore, we examined mitochondrial accumulation of Parkin using lower CCCP concentrations (0.1, 1, 5, or 10 μmol/L). In coimmunoprecipitation experiments, CCCP exposure induced ubiquitinated Parkin accumulation in the mitochondria in a dose-dependent manner in Huh7 cells, as described previously,[13] but did not induce these changes in JFH1-Huh7 cells (Figure 2D). These results suggest that

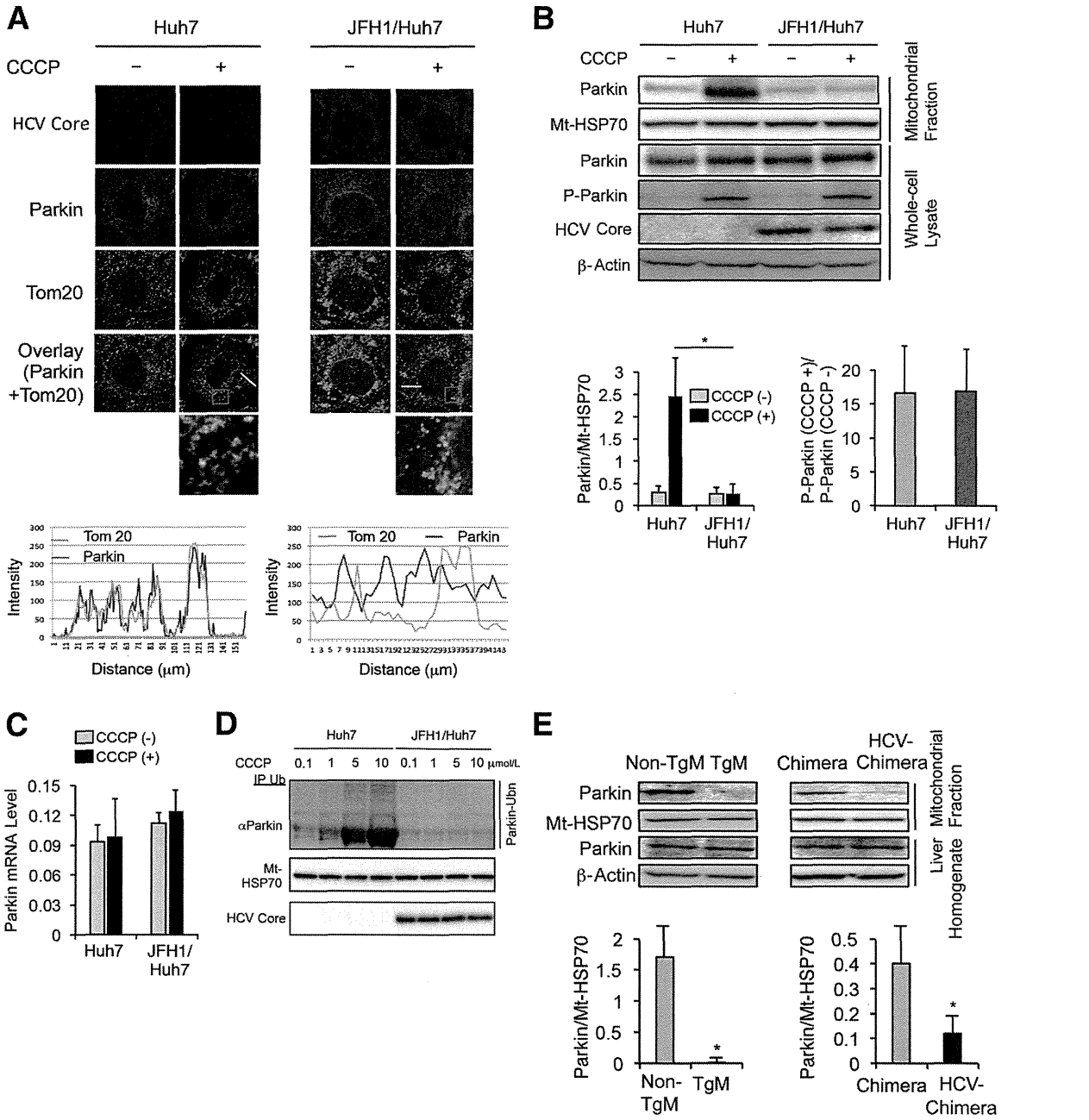

Figure 2 Effect of HCV on the translocation of Parkin to the mitochondria. **A:** Immunofluorescence staining for Parkin (red) and the mitochondrial marker Tom20 (green) in Huh7 and JFH1-Huh7 cells before (−) and after (+) carbonyl cyanide *m*-chlorophenylhydrazone (CCCP) treatment for 1 hour. **Boxed areas** are enlarged below. Endogenous Parkin that colocalizes with the mitochondria (yellow spots). Line scans indicate the colocalization of Parkin with the mitochondria and correlate to the **white lines** in the images. **Boxed areas** are enlarged below. **B:** Immunoblots for Parkin and phosphorylated Parkin (p-Parkin) using the mitochondrial fractions and whole cell lysates before and after CCCP treatment ($n = 5$). Parkin expression level was normalized to mitochondrial heat shock protein 70 (Mt-HSP70). The degree of phosphorylation was expressed as the ratio of phosphorylated Parkin after CCCP treatment to that prior treatment. **C:** Parkin mRNA level in Huh7 cells and JFH1-Huh7 cells before and after CCCP treatment ($n = 5$). The expression level for Parkin was normalized to GAPDH. **D:** Coimmunoprecipitation reveals more ubiquitinated Parkin in CCCP dose-dependent manner in Huh7 cells but not in JFH1-Huh7 cells. **E:** Immunoblots for Parkin using mitochondrial fractions of the livers or liver homogenates from non-TgM and TgM and from chimeric mice with or without HCV infection ($n = 5$ for each type of mouse). $^*P < 0.05$.

CCCP specifically induces mitophagy in Huh7 cells and that the HCV infection has an inhibitory effect on mitophagy in JFH1-Huh7 cells.

FL-N/35-transgenic mice and HCV-infected chimeric mice also showed reduced Parkin expression in the mitochondrial fraction of the liver with no change in Parkin expression levels in whole liver homogenates (Figure 2E). Serum human albumin levels, which serve as useful markers for the extent of replacement with human hepatocytes, were 16.0 ± 7.2 mg/mL in chimeric mice with HCV infection and 11.9 ± 1.7 mg/mL in chimeric mice without HCV infection (Figure 3A). These findings suggest that there was

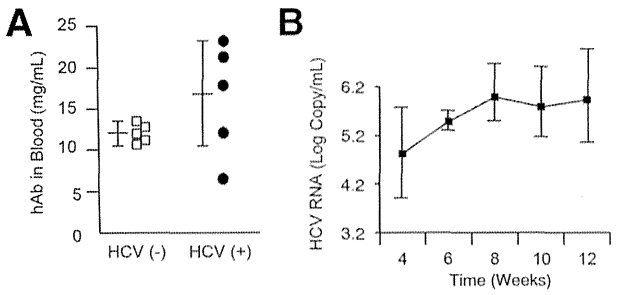

Figure 3 Human albumin and HCV RNA levels in the serum of chimeric mice with or without HCV infection. **A:** Human albumin (hAb) levels in the serum of 3-month-old chimeric mice with or without HCV infection. **B:** Serial change in HCV RNA levels in the serum after HCV infection in chimeric mice ($n = 5$).

a replacement index of >90% according to a graph of the correlation between these two parameters identified in a previous study.[25] Moreover, serum HCV RNA levels increased after infection with HCV (Figure 3B). HCV infection also suppressed the translocation of Parkin to the mitochondria in human hepatocytes.

Interaction between Parkin and the HCV Core Protein

A loss of $\Delta\Psi$ stabilizes the mitochondrial accumulation of PINK1, and PINK1 recruits Parkin from the cytoplasm to depolarized mitochondria via its kinase activity.[11–15] We confirmed that Parkin was phosphorylated to the same degree after CCCP treatment regardless of HCV infection. Therefore, we next examined the mitochondrial accumulation of PINK1. Our results indicate that PINK1 accumulated in the mitochondrial fraction after CCCP treatment, and PINK1 expression levels in whole cell lysates were comparable irrespective of HCV infection (Figure 4A). In addition, blocking PINK1 protein expression with siRNA (Figure 4B) strikingly suppressed Parkin phosphorylation (Figure 4C) and the mitochondrial Parkin signal after CCCP treatment in Huh7 cells (Figure 4D), indicating that PINK1 recruits Parkin from the cytoplasm to depolarized mitochondria via its kinase activity. Suppressed translocation of Parkin to the mitochondria by HCV infection was also confirmed after treatment with valinomycin, a K^+ ionophore that rapidly dissipates $\Delta\Psi$[32] (Figure 4E).

We next examined the association between HCV protein and Parkin and hypothesized that HCV proteins may suppress Parkin translocation to the mitochondria. Coimmunoprecipitation experiments revealed that Parkin associated with the HCV core protein but not other HCV proteins, such as NS3, NS4A, and NS5A, regardless of CCCP treatment (Figure 5A). These results suggest that the HCV core protein specifically suppressed Parkin translocation to impaired mitochondria by interacting with Parkin.

Finally, we investigated which specific Parkin domain is critical for the interaction with the HCV core protein. The proposed Parkin architecture consists of an N-terminal ubiquitin-like domain, a really interesting new gene (RING) 0 domain (RING0), and a C-terminal in-between RING domain[33] (Figure 5B). Of these domains, the RING0 domain and a complete carboxy-terminal RING configuration are critical for the translocation of Parkin to damaged mitochondria and for consequent mitophagy.[13] By using the HCV core protein as bait and either an N-terminal fragment of Parkin, including RING0 (designated Parkin 1 to 215), or a C-terminal fragment of Parkin, not including RING0 (designated Parkin 216 to 465) as prey, a Yeast Two-Hybrid assay identified a specific interaction between Parkin 1 to 215 and the HCV core protein, which was visualized as a strong blue color (activation of the *MEL1* gene encoding

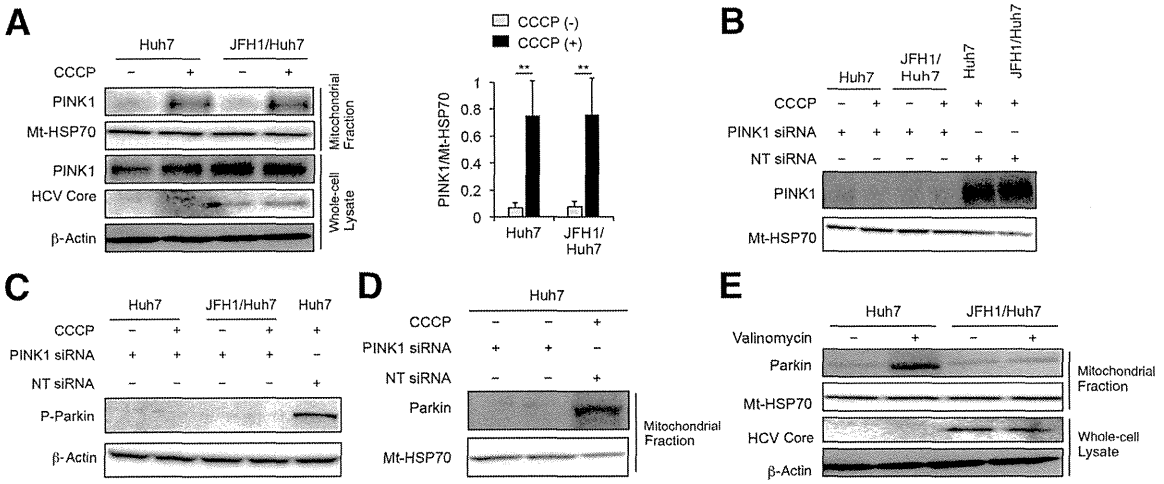

Figure 4 Mitochondrial accumulation of PINK1 after carbonyl cyanide *m*-chlorophenylhydrazone (CCCP) treatment and effect of PINK1 silencing on phosphorylation and mitochondrial translocation of Parkin. **A:** Immunoblots for PINK1 using mitochondrial fractions or whole cell lysates of Huh7 and JFH1-Huh7 cells before and after CCCP treatment ($n = 5$). Immunoblots for PINK1 using mitochondrial fractions (**B**), for phosphorylated Parkin (P-Parkin) using whole cell lysates (**C**), and for Parkin using mitochondrial fractions (**D**) of Huh7 and/or JFH1-Huh7 cells before and after CCCP treatment with or without an siRNA-mediated blockade of PINK1 expression. **E:** Immunoblots for Parkin using the mitochondrial fractions of Huh7 and JFH1-Huh7 cells before and after a 3-hour valinomycin treatment. $^{**}P < 0.01$. Mt-HSP70, mitochondrial heat shock protein 70; NT siRNA, nontargeting siRNA.

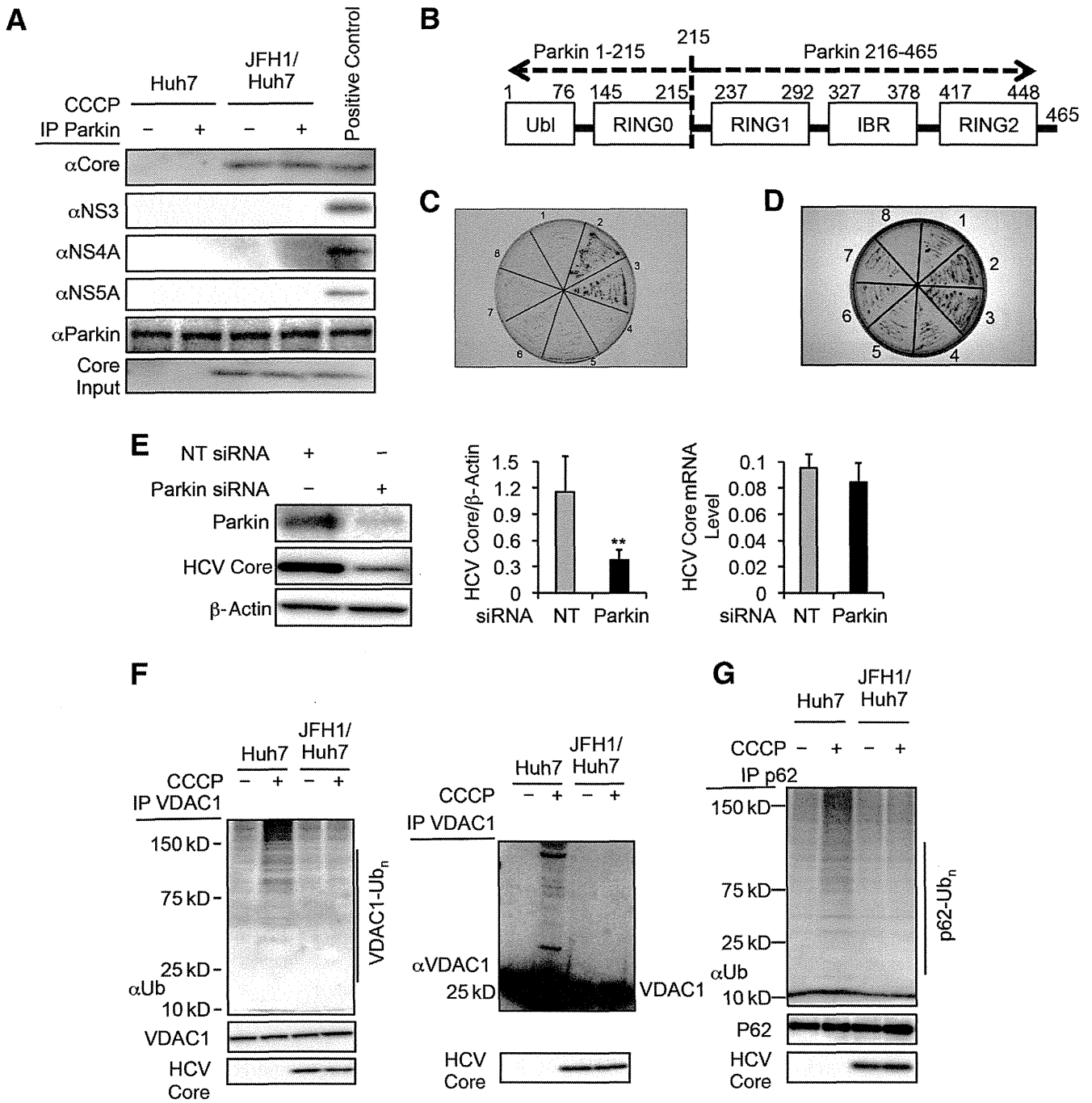

Figure 5 Interaction between Parkin and HCV core protein, effect of Parkin silencing on HCV replication, and reduction of mitochondrial outer membrane ubiquitination. **A:** Coimmunoprecipitation reveals a specific interaction of Parkin with the HCV core protein. **B:** The proposed Parkin architecture and a schematic diagram of Parkin domains. **C** and **D:** A Yeast Two-Hybrid assay identifies a specific interaction between Parkin 1 to 215 and the HCV core protein. The bait and prey for each section (1 to 8) in **C** are as follows: 1, none and none; 2, p53 and large T antigen (positive control); 3, HCV core and Parkin 1 to 215; 4, HCV core and Parkin 216 to 465; 5, HCV core and none; 6, none and Parkin 1 to 215; 7, none and Parkin 216 to 465; 8, no yeast. The bait and prey for each section in **C** were reversed in **D. E:** The HCV core protein and HCV core mRNA levels in JFH1-Huh7 cells with or without an siRNA-mediated blockade of Parkin expression ($n = 5$). **F:** Coimmunoprecipitation reveals more VDAC1 ubiquitination in Huh7 cells after carbonyl cyanide m-chlorophenylhydrazone (CCCP) treatment. Various sizes of VDAC1 immunoprecipitates are also detected by immunoblotting using an anti-VDAC1 antibody in Huh7 cells after CCCP treatment. **G:** Coimmunoprecipitation reveals more p62 ubiquitination in Huh7 cells after CCCP treatment. $^{**}P < 0.01$. IBR, in-between RING; NT, nontargeting siRNA; Parkin, Parkin-targeting siRNA; Ubl, ubiquitin-like.

α-galactosidase) (Figure 5C). In contrast, Parkin 216 to 465 did not interact with the HCV core protein. The same results were found when the core protein was used as prey and different domains of Parkin were used as bait (Figure 5D), indicating that this interaction between the two proteins was nonpolar. A previous mutational analysis of Parkin revealed that soluble Parkin mutants K211N, T240R, and G430D do not translocate to the mitochondria.[13] Although we have not

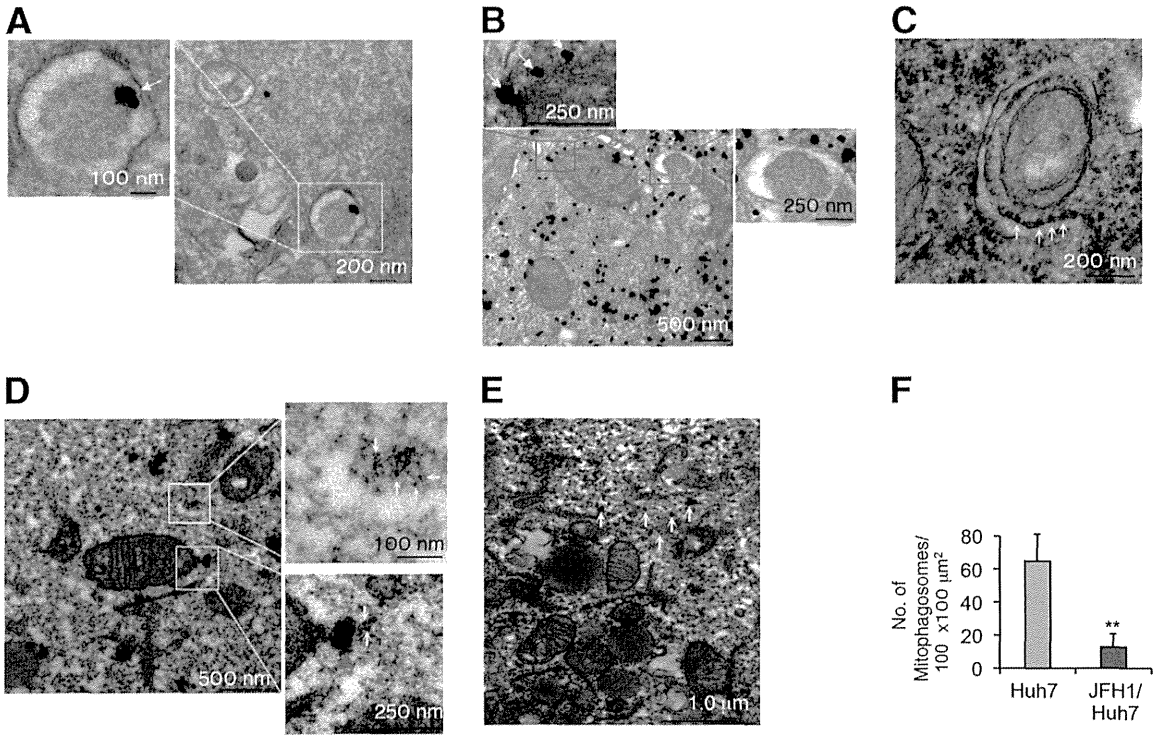

Figure 6 Electron microscopy of Huh7 cells and JFH1-Huh7 cells after carbonyl cyanide *m*-chlorophenylhydrazone (CCCP) treatment. **A–E:** Electron micrographs. **Boxed areas** are enlarged on left (Huh7 cell; **A**), above and on the right (Huh7 cell; **B**), and on the right (JFH1-Huh7 cell; **D**). The **arrows** indicate Parkin labeled with gold on the mitochondrial outer membrane (**A** and **B**), LC3 protein labeled with diaminobenzidine (DAB) on elongating isolation membrane that sequesters a single mitochondrion (Huh7 cells; **C**), Parkin core (**D**), and Parkin labeled with gold (JFH1-Huh7 cell; **E**). The **arrowheads** indicate Parkin labeled with gold (**B**) and HCV core (**D**). **F:** The number of mitophagosomes per 100 × 100 μm^2 was calculated for four randomly selected views. $^{**}P < 0.01$.

determined whether the HCV core protein binds to the region that includes lysine (K) 211 in the RING0 domain, the specific interaction of Parkin 1 to 215 with the HCV core protein raises the possibility that the core protein inhibits Parkin translocation to the mitochondria by affecting lysine 211.

After we confirmed the specific interaction between the HCV core protein and Parkin, we investigated whether Parkin affects HCV replication to investigate the functional role of the interaction between both proteins in the HCV infectious process. Parkin silencing significantly inhibited HCV replication, as indicated by a decrease in HCV core protein expression, but did not affect HCV core mRNA levels (Figure 5E). These results suggest that the association of the HCV core protein with Parkin plays a functional role in HCV propagation, although further studies are required to clarify the mechanisms.

Suppressed Ubiquitination of the Mitochondrial Outer Membrane Protein VDAC1

The next step in mitophagy after Parkin translocation to the mitochondria is the ubiquitination of mitochondrial outer membrane proteins.[13,16] Coimmunoprecipitation experiments revealed that various sizes of ubiquitinated VDAC1 species in the mitochondrial outer membrane[13] were present after CCCP treatment in Huh7 cells but not in JFH1-Huh7 cells (Figure 5F). Western blot analysis of VDAC1 immunoprecipitates revealed various sizes of VDAC1 species after CCCP treatment in Huh7 cells but not in JFH1-Huh7 cells (Figure 5F). The autophagic adaptor p62 aggregates ubiquitinated proteins by polymerizing with other p62 molecules.[13] Similarly, coimmunoprecipitation experiments revealed that CCCP treatment induced various sizes of ubiquitinated p62 species in Huh7 cells but not in JFH1-Huh7 cells (Figure 5G). These results suggest that HCV infection inhibited the Parkin-induced ubiquitination of the depolarized mitochondria.

Suppressed Mitophagosome Formation

During mitophagy, the isolation membrane sequesters a single mitochondrion or a cluster of mitochondria to form an autophagosome (mitophagosome). A single mitochondrion with Parkin on its outer membrane was sequestered by the isolation membrane after CCCP treatment in Huh7 cells (Figure 6A). Parkin in close proximity to the mitochondria and association of Parkin with mitochondrial outer membrane were observed more frequently in Huh7 cells than in JFH1-Huh7 cells (Figure 6, B, D, and E). In addition, LC3 was present on elongating isolation membrane that sequesters a single mitochondrion after CCCP treatment in Huh7 cells (Figure 6C). The number of mitophagosomes, calculated as the number of autophagosomes that contain

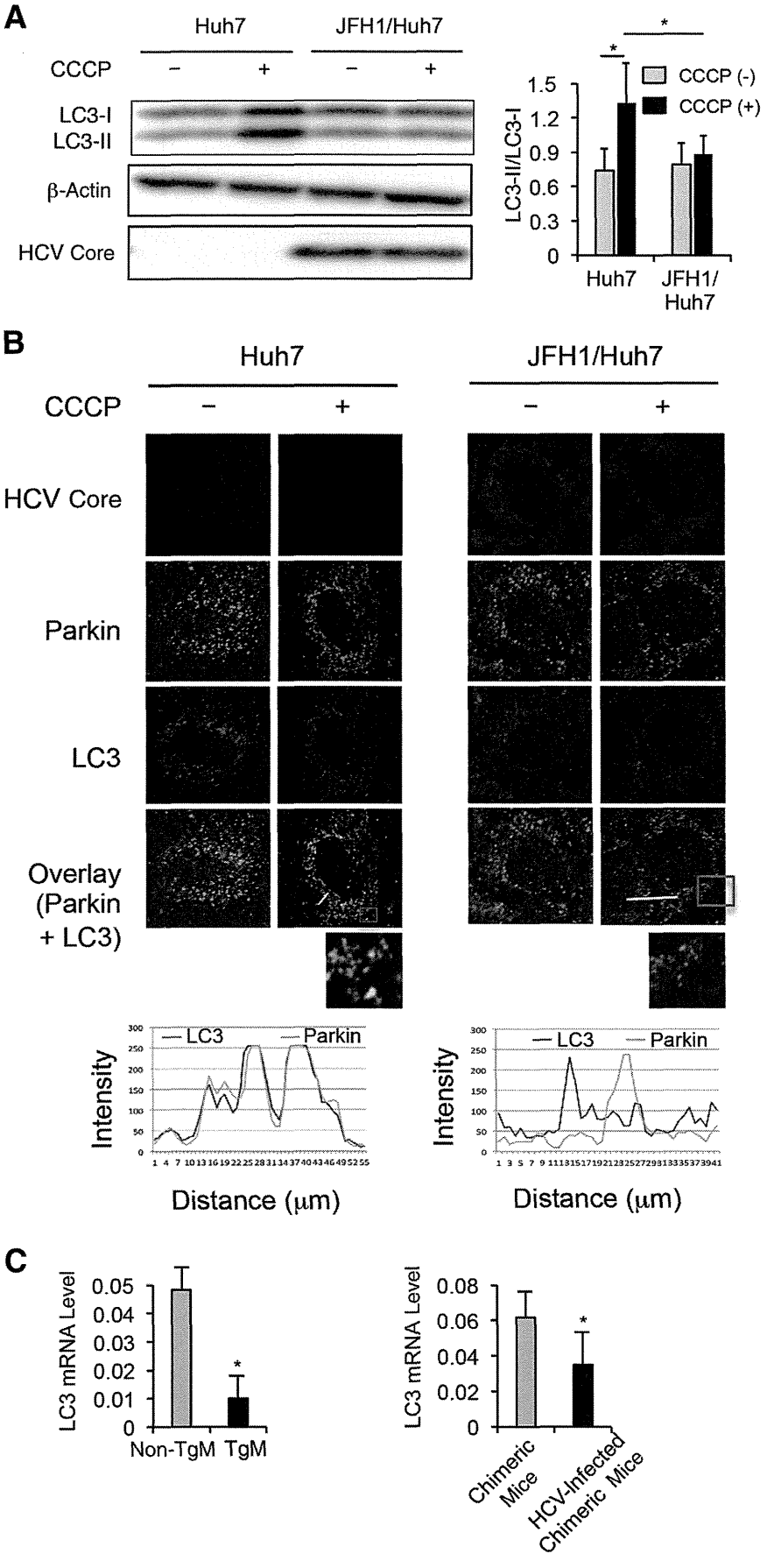

Figure 7 Effect of HCV infection on LC3-II expression and colocalization of Parkin with LC3 after carbonyl cyanide *m*-chlorophenylhydrazone (CCCP) treatment. **A:** Immunoblots for LC3-I and LC3-II using whole cell lysates of Huh7 and JFH1-Huh7 cells before and after CCCP treatment ($n = 5$). **B:** Immunofluorescence staining for Parkin (green) and LC3 (red) in Huh7 and JFH1-Huh7 cells before and after a 1-hour CCCP treatment. **Boxed areas** are enlarged below. Endogenous Parkin that colocalizes with LC3 (yellow spots). Line scans indicate the colocalization of Parkin with LC3 and correlate to the white lines in the images. **C:** The expression of LC3 mRNA in the liver from non-transgenic (non-TgM) and TgM mice ($n = 5$) and from chimeric mice without or with HCV infection ($n = 5$). The expression level of LC3 mRNA was normalized to GAPDH. $^*P < 0.05$.

mitochondria, was significantly reduced in JFH1-Huh7 cells compared with Huh7 cells (Figure 6F). Therefore, HCV infection clearly suppressed mitophagosome formation.

In agreement with suppressed mitophagosome formation, the LC3-II/I ratio was significantly lower after CCCP treatment in JFH1-Huh7 cells compared with Huh7 cells (Figure 7A), although the LC3-II/I ratio itself increased after CCCP treatment regardless of HCV infection. LC3 has been shown to be present in both complete autophagosomes and elongating isolation membranes that contain mitochondria ubiquitinated by Parkin. The present results indicate that Parkin colocalized with LC3 after CCCP treatment in Huh7 cells, whereas colocalization of Parkin and LC3 was significantly reduced in JFH1-Huh7 cells (Figure 7B). *In vivo*, FL-N/35-transgenic mice and HCV-infected chimeric mice also showed significantly reduced expression levels of LC3 mRNA in the liver compared with the control mice (Figure 7C), in agreement with reduced expression of Parkin in the mitochondrial fraction. These results may seem to be inconsistent with increased protein level of LC3-II after CCCP treatment *in vitro*. However, the lower LC3-II/I ratio after CCCP treatment in HCV-infected cells than in noninfected cells may reflect reduced expression levels of LC3 mRNA in FL-N/35-transgenic mice and HCV-infected chimeric mice. Further studies are required to clarify the mechanisms.

Several previous studies have proposed that autophagosome accumulation is enhanced on HCV infection and in HCV replicon cell lines.[34–38] Our findings of a decreased LC3-II/I ratio in JFH1-Huh7 cells, FL-N/35-transgenic mice, and HCV-infected chimeric mice seemingly contradict these previous reports. To clarify whether the decrease in LC3-II/I ratio observed in the present study indicated that macroautophagy (generally referred to as autophagy) or mitophagy was inhibited, we investigated LC3-II/I ratio in JFH1-Huh7 and Huh7 cells using Earle's balanced salt solution (EBSS) as a macroautophagy inducer (via amino acid starvation).[39] Interestingly, JFH1-Huh7 cells showed significantly increased LC3-II/I ratio compared with Huh7 cells after incubation with EBSS for 1 hour (Figure 8A), suggesting that HCV infection promoted autophagy under macroautophagy-inducible conditions. In agreement with increased LC3-II/I ratio, electron microscopy revealed that the number of autophagosomes was significantly greater after EBSS treatment in JFH1-Huh7 cells than in Huh7 cells (Figure 8B). Taken together with these results, the decrease in LC3-II/I ratio observed after CCCP treatment in JFH1-Huh7 cells likely represents a consequence of mitophagy inhibition, but not autophagy inhibition by HCV infection.

Suppression of Autophagic Degradation

The autophagic adaptor p62 can both aggregate ubiquitinated proteins by polymerizing with other p62 molecules and recruit ubiquitinated cargo into mitophagosomes by

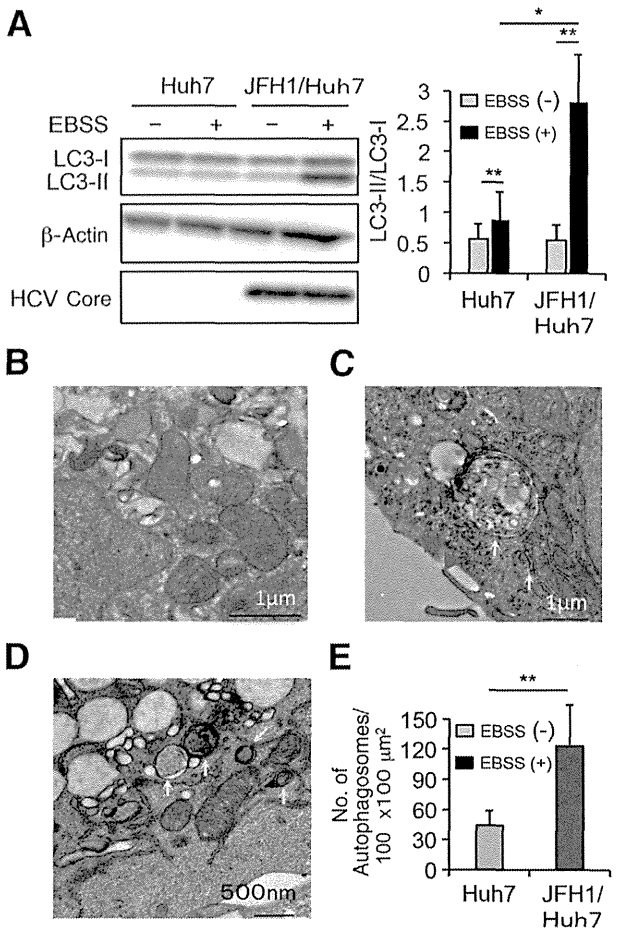

Figure 8 Effect of HCV infection on LC3-II expression and autophagosome formation after culture with Earle's balanced salt solution (EBSS). **A:** Immunoblots for LC3-II using Huh7 and JFH1-Huh7 cells before (−) and after (+) culture with EBSS ($n = 6$). The LC3-II and LC3-I expression level was normalized to β-actin. Electron microscopy of Huh7 (**B**) and JFH1-Huh7 (**C** and **D**) cells after EBSS treatment. The **arrows** indicate autophagosomes; **arrowheads**, HCV core protein. **E:** The number of autophagosomes per 100 × 100 μm^2 was calculated for five randomly selected views. $^*P < 0.05$, $^{**}P < 0.01$.

binding to LC3-II.[13] Therefore, p62 accumulation can be attributed to a deficit in autophagic degradation activity. After a 1- or 2-hour CCCP treatment, there was a smaller decrease in p62 in JFH1-Huh7 cells compared with Huh7 cells (Figure 9A). *In vivo*, FL-N/35-transgenic mice and HCV-infected chimeric mice also showed p62 accumulation in the liver compared with the control mice (Figure 9B). These results suggest that the degradation of damaged mitochondria was suppressed in the presence of HCV infection.

Finally, we assessed the change in VDAC1 content after CCCP treatment to obtain additional evidence as to whether mitophagy itself was suppressed by HCV infection. After a 2-hour CCCP treatment, a decrease in cellular content of VDAC1 was significantly smaller in JFH1-Huh7 cells than in Huh7 cells (Figure 9C). We also found that CCCP-induced increase in ROS production was greater in